Wnt and BMP signaling enhance melanocyte regeneration and suppress melanoma cell migration

Esra Katkat [1,2,#], Yeliz Demirci [1,2,3,#], Guillaume Heger [4], Irene Papatheodorou [5], Alvis Brazma [5] and Gunes Ozhan [1,2,*]

[1] Izmir Biomedicine and Genome Center (IBG), Dokuz Eylul University Health Campus, Inciralti-Balcova, 35340 Izmir, Turkey

[2] Izmir International Biomedicine and Genome Institute (IBG-Izmir), Dokuz Eylul University, Inciralti-Balcova, 35340 Izmir, Turkey

[3] Current Address: Wellcome Sanger Institute, Hinxton, Cambridge CB10 1SA, UK

[4] École Centrale de Nantes, Nantes, France

[5] European Molecular Biology Laboratory – European Bioinformatics Institute (EMBL-EBI), Cambridge, United Kingdom

Running title: Melanocyte regeneration and melanoma

Keywords: Wound healing, proliferation, differentiation, zebrafish, melanoma, nevus, comparative transcriptome analysis

[#]These authors contributed equally to this work.

[*]**Corresponding Author:**

Gunes Ozhan

Tel: +90-232 299 41 56

gunes.ozhan@ibg.edu.tr

ABSTRACT

Tissue regeneration and cancer share remarkable features including activation of cell proliferation and migration. Yet, tumors considerably differ from the regenerating tissue with respect to abnormal proliferation, invasive growth and metastasis. Thus, it is likely that cancer resembles early stages of regeneration with increased proliferation, but separates from the later stages with reduced proliferation and enhanced differentiation. Here, by exploiting the zebrafish melanocytes that can efficiently regenerate and be induced to undergo malignant melanoma, we unravel the transcriptome profiles of the regenerating melanocytes during early and late regeneration, and the melanocytic nevi and malignant melanoma. Our global comparison of the gene expression profiles of melanocyte regeneration and nevi/melanoma uncovers opposite regulation of Wnt and BMP signaling pathways between regeneration and cancer. Functional inhibition of canonical Wnt or BMP pathways during melanocyte regeneration impeded the regenerative capacity of the melanocytes. In contrast, activation of either pathway significantly promoted melanocyte regeneration and potently suppressed migration of human melanoma cells. Therefore, mechanisms of regeneration can be exploited to correct dysregulated molecular pathways and malignant transformation in cancer.

Introduction

The regenerative response of animals to damaged or lost tissues in injury or disease can occur through distinct routes including activation of resident stem cells, direct proliferation of differentiated cells and dedifferentiation of cells. These routes all involve stimulation of cell proliferation, which is also tightly associated with cancer. Cell proliferation has long been proposed to be a major event that links regeneration and tumorigenesis, with the assertion of "individuation fields" both as developing regions where organizers can rearrange the tissues to become a complete embryo and as regulators of tissue growth in the adult organisms (Waddington 1935, Stern 2000). The presence of these fields in adult organisms with high regenerative potential such as urodeles and larval anurans may argue that tissues escaping from the organizing pattern of the fields could grow into cancer (Waddington 1935). Under normal conditions, regeneration follows a common route of injury-induced events that include cell proliferation, migration, differentiation and morphogenesis to restore tissue integrity and function (King and Newmark 2012). Most importantly, these events are terminated in a controlled manner to prevent malignant transformation of the tissue (Gurtner, Werner et al. 2008, Eming, Martin et al. 2014, MacCarthy-Morrogh and Martin 2020). However, abnormal progression of regeneration could convert the healing tissue into a rapidly proliferating tumor that fails to establish tissue integrity (Haddow 1972, Coussens and Werb 2002, Beachy, Karhadkar et al. 2004, Gurtner, Werner et al. 2008, Schafer and Werner 2008, Oviedo and Beane 2009). In addition to the elevated levels of cell proliferation, clinical observations such as ulceration and tumor formation during abnormal wound repair, activation of inflammatory response, angiogenesis and differential expression of genes involved in cell proliferation, survival and migration have supported the hypothesis that proposes cancers as non-healing wounds (Dolberg, Hollingsworth et al. 1985, Riss, Khanna et al. 2006, Schafer and Werner 2008, DiPietro 2013, Crusz and Balkwill 2015, Dvorak 2015, DiPietro 2016, Karin and Clevers 2016). These observations thus rationalize a potential link between regeneration and cancer. Nevertheless, the underlying mechanistic link between the two phenomena has been mostly overlooked at the molecular level as regard to genome-wide analysis and comparison of gene expression in regenerating tissue and cancer tissue.

The first molecular evidence that associate cancer and regeneration were obtained from the studies performed in urodele amphibians and planarians (Seilern-Aspang and Kratochwill 1962, Hall, Morita et al. 1986, Agata and Watanabe 1999, Sanchez Alvarado and Tsonis 2006, Brockes and Kumar 2008). For example, the newt limb, where amputation at the site of tumor induction results in regeneration of a normal limb without any tumors, serves as a unique model showing that regeneration indeed has the capacity to correct malignant transformation (Cajal 1928, Rose and Wallingford 1948, Rose and Rose 1952, Tsonis 1983). Interestingly, regeneration and cancer studies conducted on newt, salamander and axolotl showed that body regions such as limbs and tails with high epimorphic regeneration capacity exert resistance to tumor induction when compared to body sites with low regeneration capacity. These results again support Waddington's theory of organizers where cells in the individuation fields are less susceptible to turn into a malignant tissue (Foster 1963, Tsonis 1983). However, whether the tissue would achieve complete regeneration or become cancerous is tightly dependent on how growth is controlled in these regenerative fields (Waddington 1935, Stern 2000). Therefore, these observations raise the questions of whether the regenerative fields develop intrinsic resistance to cancer formation and whether regeneration could indeed be a good starting point to correct malignant transformations.

Melanocytes constitute a heterogeneous group of melanin-producing cells with diverse roles from pigmenting the skin and providing it with protection against UV damage to neuroendocrine functions (Takeda, Takahashi et al. 2007, Plonka, Passeron et al. 2009). Adult melanocytes belong to the skin, which is the largest and one of the most regenerative organs in vertebrates. Studies on physiological regeneration of mammalian hair follicles have proven that melanocytes are derived from melanocyte stem cells (MSCs), which are capable of self-renewal and fully competent to produce mature melanocytes (Oshima, Rochat et al. 2001, Nishimura, Jordan et al. 2002, White and Zon 2008). Microphthalmia-associated transcription factor (Mitf), Endothelin receptor B (Ednrb), c-Kit, Notch and Wnt signaling pathways have been found to play important roles in maintenance of MSCs and melanocyte regeneration in adulthood (Rawls and Johnson 2001, McGill, Horstmann et al. 2002, Kumano, Masuda et al. 2008, O'Reilly-Pol and Johnson 2013, Iyengar, Kasheta et al. 2015, Guo, Xing et al. 2016, Takeo, Lee et al. 2016, Watanabe, Motohashi et al. 2016). Importantly, the biological

processes and pathways including Mitf, Ednrb, c-Kit and Notch that are characteristic of melanocyte regeneration have also been associated with melanoma, the most aggressive and deadliest form of skin cancer originating from the melanocyte lineage (Sulaimon and Kitchell 2003, Widlund and Fisher 2003, White and Zon 2008, Krauss, Frohnhöfer et al. 2014, Liu, Fukunaga-Kalabis et al. 2014, Wang, Liu et al. 2018). The origin of melanoma could be either *de novo* transformation of melanocytes or congenital/inherited nevi (Garbe, Peris et al. 2016, Yeh and Bastian 2021). 8-12% of all melanomas have been linked with a germline mutation or deletion of the tumor suppressor gene *cyclin-dependent kinase inhibitor 2A* (*cdkn2a*), causing aberrant regulation of the cell cycle (Fountain, Karayiorgou et al. 1992, Serrano, Hannon et al. 1993, Schmidt, Ichimura et al. 1997, Gruber, Kastelan et al. 2008). Here, we postulate that the molecular mechanisms of tumorigenesis should show more parallelism with those of regeneration at its relatively earlier stages. Yet, the mechanisms could differ later when regeneration is successfully completed but cancer cells continuously proliferate. Thus, it is rational to assume that while the early-expressed genes are more commonly shared between the two phenomena, late-expressed genes rather differ. To address this assumption, on the one side, we have generated an adult zebrafish model of melanocyte regeneration and examined different stages of regeneration quantitatively for the expression of proliferation and differentiation markers. Accordingly, we determined 1-day post-ablation (dpa) as the "proliferative or early regeneration stage" and 7 dpa as the "differentiation or late regeneration stage". Comparative genome-wide transcriptome profiling of the regenerating melanocytes in the caudal fin, which we selected as a common platform for comparative analysis of differentially expressed genes (DEGs), revealed that 1 dpa and 7 dpa are transcriptionally distinct stages of melanocyte regeneration. On the other side, we have generated an adult zebrafish model of melanoma by exploiting the *Tg(mitfa+/-;kita-GFP-RAS*^{G12V}*)* line that enabled the characterization of both melanocytic nevi and malignant melanoma. Transcriptome analysis demonstrated that nevi and melanoma shared DEGs related to melanocyte differentiation and pigmentation but separated from each other by the genes associated with proliferation and neural crest cell (NCC) signature. 1 dpa and melanoma were mostly enriched for cell cycle and DNA replication signatures, which were absent in 7 dpa, indicating that the early stage of melanocyte regeneration and malignant melanoma have similar transcriptional profiles. In contrast, 7 dpa is hallmarked by the activation of melanocyte differentiation and pigmentation genes.

By globally comparing the transcriptomes of the early and late melanocyte regeneration stages to those of nevi and melanoma, we found that Wnt and BMP signaling pathways were oppositely regulated between melanocyte regeneration and melanoma. While inhibition of canonical Wnt or BMP pathways suppressed the regenerative capacity of the melanocytes, their activation significantly enhanced melanocyte regeneration and hindered the migration of melanoma cells. Overall, by unraveling the stage-dependent alterations in gene expression profiles and the capabilities of molecular pathways between melanocyte regeneration and melanoma, our study pioneers for testing the potential of adapting the gene expression programs of cancer cells to those of regenerating cells to stop cancer progression.

Materials and Methods

Zebrafish husbandry and maintenance

Zebrafish are maintained in accordance with the guidelines of the Izmir Biomedicine and Genome Center's Animal Care and Use Committee. All animal experiments were performed with the approval of the Animal Experiments Local Ethics Committee of Izmir Biomedicine and Genome Center (IBG-AELEC).

Generation of the adult zebrafish model of melanocyte regeneration

The zebrafish melanocyte regeneration model was generated by using Neocuproine (NCP; Sigma-Aldrich, MO, USA), a copper chelating agent that specifically kills mature melanocytes without giving harm to *mitf*+ melanocyte progenitor cells (O'Reilly-Pol and Johnson 2008). Melanocytes are sensitive to copper depletion as copper is a cofactor for tyrosinase (Tyr), the catalyzer of melanin synthesis (Akyilmaz, Yorganci et al. 2010). 6-12 month-old wild-type (wt) AB zebrafish were treated with 1 µM of NCP for 24 hours and caudal fins were collected at 1, 2, 3, 4, 7, 15 and 20 days post-ablation (dpa) (Figure 1, left; Figure S1A). Samples from 1, 2, 3 and 4 dpa and samples from 7, 15 and 20 dpa were assayed for early and late melanocyte regeneration, respectively. First, fish were anesthetized with 10 mg/mL of Tricaine (MilliporeSigma, MA, USA). Following immobilization, the caudal fin of each fish was resected to 50% of their original size along the dorsoventral axis with a razor blade and stored in RNAlater until RNA isolation. Four animals were used for each regeneration stage.

Generation of the adult zebrafish model of melanoma

The melanoma model was generated as described previously (Santoriello, Gennaro et al. 2010). First, a Tg(*mitfa-/-; kita:GFP-RAS*^{G12V}) zebrafish line was generated by outcrossing the homozygous *kita:GFP-RAS*^{G12V} line to the *nacre (mitfa-/-)* mutant, which is devoid of melanocytes due to a loss-of-function mutation in *mitfa* gene (Lister, Robertson et al. 1999). Next, the Tg(*mitfa-/-; kita:GFP-RAS*^{G12V}) line was outcrossed to the wt (AB) zebrafish to generate 50% *Tg(mitfa+/-; kita-GFP-RAS*^{G12V}*)* embryos that could generate melanocytes due to the single functional copy of *mitfa* and expressed *RAS*^{G12V} oncogene only in the melanocytes due to the *kita* promoter, leading to hyperpigmentation throughout the body (Figure 1, right). The remaining 50% of embryos were Tg(*mitfa+/-*) and appeared as wt.

Melanocyte regeneration assay on zebrafish embryos/larvae

Dechorionated wt (AB) zebrafish embryos were treated with 20 µM 4-Hydroxyanisole (4-HA, Sigma-Aldrich, MO, USA) in embryo water between 36 hours post-fertilization (hpf) and 60 hpf to ablate melanocytes and induce melanocyte regeneration. 4-HA is a phenolic compound that is converted to a toxic form of o-quinine in melanocytes, eventually leading to their death (Yang and Johnson 2006). 4-HA-treated larvae at 2 days post-fertilization (dpf) were then incubated with the drugs (see below) that activate or inhibit the signaling pathways determined according to the analysis results of the RNA sequencing data. 2 dpf larvae were aligned in a 24-well plate (10 larvae/well, 60 larvae/group) and melanocyte regeneration was quantified daily until 7 dpf. Drugs were replenished every other day.

Cell culture

The human melanoma cells SK-MEL-28 (HTB-72™) were cultured in Dulbecco's modified eagle medium (DMEM) supplemented with 10% fetal bovine serum (FBS) and 1% Pen/Strep at 37°C in 5% (v/v) CO_2 humidified environment. On the day of injection, approximately 1.5 x 10^6 cells were harvested at 70-80% confluence and washed with Dulbecco's phosphate buffered saline (DPBS) containing 10% FBS. Next, cells were resuspended in 50 µl of DPBS with 10% FBS and incubated with 2.5 µl of Vybrant® DiO cell-labeling solution (Invitrogen, MA, USA) for 20 min. Cells were then washed once with FBS and twice with DPBS containing 10% FBS. The pellet was then resuspended in DMEM with 10% FBS to a final density of 30.000 cells/µl. Cells were mixed with 1 µl of Phenol Red (Sigma-Aldrich, MO, USA).

Generation of zebrafish larval xenografts and migration assay

2 dpf *casper* (*roy -/-; nacre-/-)* zebrafish larvae were dechorionated by incubating in 0.1 mg/mL pronase (Sigma-Aldrich, MO, USA) solution for 10 min at 28°C. Larvae were then anesthetized with 1 mg/mL Tricaine in E3 medium and transferred to a microinjection plate prepared with 3% agarose in E3. Borosilicate glass capillaries (4 inches, OD 1.0 mm, World Precision Instruments, FL, USA) were used for injection. 3 µl of SK-MEL-28 cell suspension was loaded into the capillary needle and 400-500 cells were injected directly into the yolk sac of the larva by using a micromanipulator and a pneumatic pico-pump. Injections were gently performed into the middle of the yolk sac to avoid any damage to the duct of Cuvier. Larvae were incubated at 34°C in fresh E3 overnight. The next day, larvae showing infiltration of tumor cells into blood circulation were discarded. Larvae with injected cells in the yolk sac were kept and processed further for drug treatments. Larvae were randomly distributed to each experimental group and exposed to the drugs (see below) that activate or inhibit the signaling pathways determined according to the analysis results of the RNA sequencing data. At 5 days post-injection (dpi), xenografts were imaged and the percentage of micrometastasis was determined.

Drug administration

Stock solutions of NCP were prepared as 25 mg/ml in DMSO. The final concentrations of NCP and 4-HA were 1 µM and 16 µM, respectively. A stock solution of epinephrine (Sigma-Aldrich, MO, USA) was prepared as 18 mg/ml (1 M) by dissolving in 0.125 M HCl . Prior to imaging, zebrafish were treated with epinephrine for 15-20 min at a final concentration of 1 mg/ml. The drugs used for the embryo/larva regeneration and xenotransplantation assays were as follows: the Wnt antagonist IWR-1 (Sigma-Aldrich, MO, USA), the GSK-3 inhibitor and Wnt agonist BIO (Sigma-Aldrich, MO, USA), the selective bone morphogenetic protein (BMP) antagonist DMH-1 (Bio-Vision Inc., CA, USA) and the BMP agonist isoliquiritigenin (ISL; Raybiotech, GA, USA). Toxicity tests were conducted on zebrafish embryos that were treated with different concentrations of the drugs from 24 hpf to 7 dpf. Based on a survival rate above 90%, the working concentrations of drugs were determined as follows: 10 µM IWR-1, 1 µM for BIO, 20 µM for ISL and 5 µM for DMH-1. DMSO was used as a control.

In vivo imaging and quantification

Zebrafish larvae were anesthetized with 1 mg/ml Tricaine, transferred to a 6-well glass-bottom plate containing 3% methylcellulose (Sigma-Aldrich, MO, USA) in E3 medium. All bright-field and

fluorescent images of the larvae were captured with an Olympus SZX2-ILLB stereomicroscope (Olympus Corporation, Japan). At 5 dpi, the percentage of the micrometastasis in the caudal tissue and the tail fin was determined using the formula given below (Martinez-Lopez, Póvoa et al. 2021):

% metastasis = (number of live xenografts with micrometastasis x 100)/total number of xenografts

Image processing and quantification were performed using the automated cell counting method of ImageJ software of Fiji. The following steps were performed to count micrometastasis in the xenograft assay: The color (RGB) image to be counted was opened in ImageJ and converted to grayscale (image>type>8-bit or 16-bit). Next, the threshold was adjusted to highlight the structures to be counted (Image>Adjust>Threshold). Background noise was subtracted (Process>Noise>Despeckle). Finally, all particles were automatically counted on the ROI (Analyze>Analyze Particles). The number of dorsal melanocytes on the head and trunk of the larva was counted (Plugins>Analyze>Cell Counter).

RNA isolation and quantitative PCR

RNAlater was removed from the fin tissues and QIAzol lysis reagent (Qiagen, Germany) was added onto the samples. Fins were weighed and validated to meet the kit requirements. The fin tissue was homogenized with RNase-free disposable pestles and the lysate was passed through an 20G insulin needle 5-10 times. RNA isolation was carried out using the RNeasy® micro kit (Qiagen, Germany) according to the manufacturer's instructions. The samples were treated with DNAse I (Qiagen, Germany) to prevent genomic DNA contamination. Total RNA concentration was determined in a NanoDrop™ 2000/C spectrophotometer (Thermo Fisher Scientific, MA, USA). RNA quality was verified using RNA 6000 Pico kit (Agilent Technologies, CA, USA) according to the manufacturer's instructions and samples were validated to have RNA integrity values above 7.0. cDNA synthesis was performed by using the iScript^{TM} cDNA synthesis kit (Bio-Rad Laboratories, CA, USA).

qPCR was performed in triplicates by using GoTaq qPCR Master Mix (Promega, WI, USA) in an Applied Biosystems 7500 Fast Real-Time PCR machine (Thermo Fisher Scientific, MA, USA). For each sample, expression values were normalized to *Danio rerio ribosomal protein L13a (rpl13a)*, the reference housekeeping gene. The efficiency of each primer pair, designed by using NCBI's Primer-BLAST, was assessed by using the standard curve assay according to the relevant program of the

machine. Standard curves were plotted for each primer pair with the 1:5, 1:25, 1:125 and 1:625 serial dilutions of the cDNA samples. Standard curves with C_T values were generated by using the ABI software and a correlation coefficient (R^2) was calculated for each primer pair. Water was used as a negative control to eliminate contamination and primer-dimer formation. Primer pairs with R^2 values equal to or greater than 0.99 and an efficiency falling in the acceptable range (90-110%) were used in the qPCR reactions. The values are indicated as mean ± SEM (Standard Error of Mean) of triplicates. Primer sequences are provided in Table S1.

Library construction and RNA sequencing (RNA-seq)

The samples with an RNA Integrity Number (RIN) ≥ 8 were selected for RNA-seq. RNA quality was also checked by performing quantitative reverse transcription PCR (RT-PCR) with a primer pair generating an 812-bp product for zebrafish *beta-actin 1* (*actb1*). The samples that passed the quality controls were sent to the Genomics Core Facility (GeneCore, EMBL, Germany) for library preparation and RNA-seq. An Illumina TruSeq RNA Library Preparation Kit v2 (Illumina, CA, USA) was used to prepare libraries according to the instructions given by the manufacturer. For each reaction, 500 ng of cDNA was used. A paired-end, strand-specific sequencing platform was used on Illumina NextSeq 500 (Illumina, CA, USA) with a read length of 75 bp.

Bioinformatics analysis

Read quality control of RNA-seq samples obtained from the zebrafish melanocyte regeneration stages (1 dpa and 7 dpa), zebrafish melanocytic nevi and zebrafish malignant melanoma was initially performed by using the FastQC tool (Andrews 2010). The reads were aligned to the zebrafish reference genome GRCz11 (danRer11) by using HISAT2 (version 2.1.0) (Kim, Langmead et al. 2015). The read summarizer HTSeq 0.6.0 was used to count transcripts by using the annotation file Danio_rerio.GRCz11.93.gtf from the Ensembl database. Gene expression counts were normalized and tested for differential expression using DESeq2 (Love, Huber et al. 2014). All genes were tested for differential expression at the two stages of melanocyte regeneration (1 dpa and 7 dpa), in nevi and in melanoma, all in contrast to the control baseline zebrafish transcriptome, using a Wald test on log2 fold changes. In all comparisons, differentially expressed genes (DEGs) were called with a false

discovery rate (FDR) of 0.1 and an effect size threshold of log2(1.2) (thereafter referred to as FC>1.2 in either direction). Gene ontology (GO) and pathway enrichment analyses were carried out with lists of all DEGs against DAVID knowledgebase (Huang da, Sherman et al. 2009). The EASE score, a modified one-tailed Fisher's exact test, was used to measure the significance of the terms' and pathways' enrichment. The data was visualized by principal component analysis (PCA) using the packages ggplot2 (version 3.3.2) and pheatmap (version 1.0.12) (Kolde 2012, Wickham 2016). Gene lists were obtained from the AmiGO (Carbon et al., 2009) and KEGG databases for selected GO terms and pathways. The enrichment of DEGs in GO terms and KEGG pathways were visualized using GOChord plots (Walter, Sanchez-Cabo et al. 2015).

Statistical analysis

The data were analyzed statistically with the GraphPad Prism 9 software (Graphpad Software Inc., CA, USA). Two-tailed Student's t-test was used for qPCR and analysis of the percentage of micrometastasis. One-way ANOVA and Tukey's multiple comparison test were used to compare more than two groups. Statistical significance was evaluated as follows: *$p \leq 0.05$, **$p \leq 0.01$, ***$p \leq 0.001$, ****$p \leq 0.0001$ and ns: non-significant.

Results

Early and late stages of melanocyte regeneration are distinguished by their expression of the proliferation and differentiation markers and their transcriptomes

The transcriptional dynamics underlying melanocyte lineage progression in the hair bulb have recently been investigated with respect to activation of quiescent MSCs to proliferate and differentiate into mature melanocytes in a mouse model (Infarinato, Stewart et al. 2020). Pigment cells including the melanocytes and iridophores have been analyzed at the transcriptional level (Higdon, Mitra et al. 2013). However, gene expression profiles of the regenerating melanocytes have not been identified at proliferation and differentiation stages so far. Thus, we set out to unravel the DEGs at the early regeneration stage, where proliferation is the prominent event, and the late regeneration stage, where proliferative response is replaced by differentiation. Initially, to determine the early and late stages of melanocyte regeneration, we ablated melanocytes of the adult zebrafish by 1-day of NCP treatment and

monitored NCP-treated zebrafish daily to track the melanocyte death, depigmentation, onset of melanocyte differentiation and reconstitution of the stripe pattern after washout (Figures 2A, S1A). We followed the change in the morphology of the melanocytes until most of the melanin content was disposed of the skin. Melanocytic aggregates began to disappear at 3 dpa and were substantially lost at 4 dpa (Figures 2A, S1A). It is important to note that, despite losing their dendritic morphologies, some melanocytic aggregates remained as black smears. Thus, we assumed that most of the melanocytes lost their cellular activity at 4 dpa. Melanocyte differentiation started all over the body at 7 dpa and the stripe pattern was reconstituted within 30 days after the fish were returned to freshwater (Figures 2A, S1A). Since 3 or 10 days of NCP treatment has been shown to exert a cytotoxic effect on most melanocytes in adult zebrafish, we treated the zebrafish with epinephrine, which leads to the assembly of melanin-containing melanosomes towards the nucleus in the presence of an epinephrine signal when they are alive (O'Reilly-Pol and Johnson 2008, Iyengar, Kasheta et al. 2015, Kang, Karra et al. 2015). Whereas the dendritic morphology of melanocytes turned into compact rounds in untreated fish within 15-20 min, melanocytes of NCP-treated fish did not respond at 1 dpa and 2 dpa, independent of their dendritic or smeary shape, confirming the successful ablation of the melanocytes (Figure S1B).

After confirming successful melanocyte ablation, we aimed to determine the early and late stages of melanocyte regeneration and isolated total RNA from caudal fin tissues collected at 1, 2, 3, 4, 7, 12 and 20 dpa. Tissue samples from four fish were pooled. For the early stage, we used the proliferation marker *proliferating cell nuclear antigen (pcna)*. Although 45% of melanocytes are directly differentiated from a set-aside population of *mitfa+* progenitors without cell division, the majority of the newly generated melanocytes stem from *mitfa+* progenitor cells via cell division (Curado, Anderson et al. 2007, Kang, Karra et al. 2015). *Proliferating cell nuclear antigen (pcna)* expression increased 4-fold at 1 dpa, abruptly decreased at 2 dpa and returned to the control levels at 7 dpa (Figure S2A). As the early strong activation of proliferation is consistent with the previous data obtained from adult melanocyte regeneration (Iyengar, Kasheta et al. 2015), we determined 1 dpa as the early stage of melanocyte regeneration. For the late stage, we exploited the master regulator of melanocyte development *mitfa* and the late melanocyte differentiation markers *dopachrome tautomerase (dct)* and *tyrosinase (tyr)* (Rawls and Johnson 2001, Curado, Anderson et al. 2007, Ceol, Houvras et al. 2008). The expression levels of

mitfa , *dct* and *tyr* started to increase at around 3 dpa, reached their peak at 7 dpa and inclined toward control levels at 12 dpa (Figure S2A). Taken together with the expression of the proliferation marker at control levels at 7 dpa, we considered 7 dpa as the late melanocyte regeneration stage. This also correlates with our track of melanocyte pigmentation at the macroscopic level where new melanocytes appeared throughout the body at 7 dpa (Figure S1A). The changes in the expression of proliferation and differentiation markers for the individual fin samples were consistent with the pooled fin samples (Figure S2B). Thus, we decided to exploit the zebrafish caudal fin, which successfully confirmed activation of the marker genes at different stages of regeneration. Next, to identify the differentially expressed genes at early and late stages of melanocyte regeneration, we collected the caudal fin tissues of the DMSO-treated and NCP-treated zebrafish (Figure 1) and performed RNA-seq. Principal component analysis (PCA) revealed that the samples of 1dpa and 7 dpa were well separated from each other and the control samples (Figure 2B). We have identified 5848 genes (2928 upregulated=Up and 2920 downregulated=Down) and 9106 genes (4127 Up and 4979 Down) that were differentially expressed in response to melanocyte ablation at 1 dpa and 7 dpa, respectively (Figure 2C-D, Table S2). Interestingly, while only 40% of the DEGs detected at 1 dpa were unique to this stage, at 7 dpa the percentage of unique DEGs increased to 61%. Together, these results indicate that 1 dpa and 7 dpa represent stages of proliferation (early) and differentiation (late), respectively and validate them as two distinct stages of melanocyte regeneration at the transcriptional level.

Early and late stages of melanocyte regeneration have distinct gene expression profiles

To understand how gene expression profiles alter throughout proliferation and differentiation stages of melanocyte regeneration, we plotted the heatmap of the expression of a group of selected genes that are involved in neural crest cell (NCC) differentiation, epithelial to mesenchymal transition (EMT), melanocyte differentiation/pigmentation, cell cycle, immune response, proliferation and stem cell differentiation (Figure 3A). The heatmap shows the normalized counts for the biological replicates. The baseline expression in control groups is used to determine the direction of regulation at 1 dpa and 7 dpa with respect to the control. A vast number of DEGs, which are associated with proliferation and cell cycle, including *pcna, cdk2, cyclin D1 (ccnd1), lysineK-specific demethylase 8 (kdm8)* and *kinetochore protein* encoding *zwilch* were Up at 1 dpa and Down at 7 dpa, in line with the high proliferative activity

at the early stage of melanocyte regeneration. Interestingly, most of the immune response-related genes appeared to be oppositely regulated at 1 dpa and 7 dpa. For example, while part of genes associated with innate immune response such as the Fas receptor gene *fas*, *fyn-related Src family tyrosine kinase (frk)* and E3 SUMO-protein ligase-encoding *pias4a* were selectively Up at 1 dpa, others including *tumor necrosis factor b (tnfb)*, *complement component 4* (*c4*) and *Src family tyrosine kinase (lck)* were selectively Up at 7 dpa (Figure 3A). Early activation of *tnfb* is supported by the rapid upregulation of its expression during photoreceptor regeneration in the adult zebrafish between 1 dpa and 2 dpa (Silva, Nagashima et al. 2020). Several neural crest-related genes including *paired box 3a (pax3a)*, *SRY-box transcription factor 8b (Sox8b)* and *SRY-box transcription factor 10 (sox10)* that are also known for their role in pigment cell development (White and Zon 2008, Mort, Jackson et al. 2015) were Down at 1 dpa but Up at 7 dpa (Figure 3A). On the other hand, *regulator of G protein signaling 2 (rgs2)* and the transcription factor-encoding gene *forkhead box D3 (foxd3)*, which act as negative regulator of neural crest development and melanocyte lineage development, respectively (Curran, Lister et al. 2010, Lin, Chiang et al. 2017), were Down at both 1 dpa and 7 dpa as compared to the control. *Rsg2* has been shown to restrict the *sox10(+)* non-ectomesenchymal lineage that acts as a source of the melanocytes (Lin, Chiang et al. 2017). Thus, selective downregulation of *rsg2* and upregulation of *sox10* at 7 dpa support the idea that melanocyte lineage regeneration is promoted at the expense of the *sox10(-)* ectomesenchymal NCC. A large number of pigmentation-related genes such as *tyr*, *dct*, *oculocutaneous albinism II (oca2)*, *premelanosome protein a (pmela)*, *endothelin 3b (edn3b)* and *tyrosinase-related protein 1a (tyrp1a)* (Cichorek, Wachulska et al. 2013) exhibited robust upregulation at 7 dpa, indicating induction of the melanocyte differentiation program at the later stage of regeneration (Figure 3A). On the other hand, at 1 dpa, these genes were Down, likely due to the high proliferative activity and suppressed differentiation.

Next to further characterize the molecular signatures that define early and late stages of melanocyte regeneration, we performed GO term enrichment analysis for 1 dpa and 7 dpa. At 1 dpa, the most significantly enriched DEGs were grouped in the biological process (BP) terms including DNA replication, DNA damage response and various DNA repair mechanisms (Figure 3B, Table S3). KEGG pathway analysis likewise revealed that, at 1 dpa, DEGs were enriched in DNA replication, cell cycle

and major DNA repair pathways (Figure S3A, Table S4). On the other hand, at 7 dpa, the DEGs were mostly enriched in GO-BP terms related to translation and RNA processing such as protein transport, protein folding, mRNA splicing and rRNA processing (Figure 3C, Table S3). Top KEGG pathways enriched at 7 dpa included protein translation, protein transport, general RNA processing, proteasome and cellular respiration, mostly overlapping with the GO terms enriched at this stage (Figure S3A, Table S4). We also validated changes in expression of the DEGs that are regulated at either 1 dpa or 7 dpa or both stages by qPCR (Figure 3D, Table S1). Thus, early and late stages of melanocyte regeneration are considerably different from each other with respect to their transcriptome profiles.

Melanoma resembles melanocytic nevi with respect to the activation of melanocyte differentiation and pigmentation but differs from nevi by the proliferative burst and oppositely regulated NCC signature

To generate the melanoma model, we exploited the *Tg(mitfa+/-;kita-GFP-RAS^{G12V})* zebrafish, which is a well-established line to investigate the transcriptional landscape from the formation of melanocytic nevi to malignant melanoma. In this line, *kita* promoter drives the mutant *RAS* oncogene expression in the melanocyte lineage to promote malignant transformation of melanocytes to melanoma within 3 months, without the need for additional inactivating mutations on tumor suppressor genes (Santoriello, Gennaro et al. 2010, Forbes, Beare et al. 2017). As we could validate the zebrafish caudal fin as a reliable model for melanocyte regeneration, we decided to include the melanoma tissue that developed only on the caudal fin. In this way, we aimed to restrict the source tissue for transcriptome analysis to the caudal fin in both regeneration and cancer and minimize potential variation that might occur across different tissues. Thus, we collected tissues of nevi and melanoma that developed in the caudal fin of *Tg(mitfa+/-;kita-GFP-RAS^{G12V})* zebrafish for RNA-seq analysis (Figure 4A). PCA exhibited a very clear distinction of the control, nevi and melanoma samples (Figure 4B). While only 1744 genes (1178 Up and 566 Down) were differentially expressed in nevi, the melanoma tissue harbored 11. 265 DEGs (5638 Up and 5627 Down) as compared to the control fin tissue (Figure 4C-D, Table S2). Not surprisingly, 87% of the DEGs detected in melanoma samples were unique to melanoma.

To further distinguish malignant melanoma from melanocytic nevi at the transcriptional level, we generated a heatmap of selected genes from among the most significant DEGs involved in

proliferation/cell cycle, NCC differentiation and melanocyte differentiation/pigmentation (Figure 5A). We detected a remarkable similarity between control and nevi samples in the expression of the majority of the selected genes that belong to proliferation and NCC differentiation groups. On the other hand, proliferation-related genes including *cdk2, minichromosome maintenance complex component 7 (mcm7), pcna, marker of proliferation Ki-67 (mki67)* and *cdk1* were dramatically Up in the melanoma tissues (Figure 5A). Moreover, the Cdk inhibitor gene *cdkn1bb*, a negative regulator of G1/S transition of mitotic cell cycle, (Chu, Hengst, & Slingerland, 2008) was Down in melanoma and at 1 dpa (Figure 5A, Table S2). Strikingly, expression of the selected NCC gene signature was completely oppositely regulated between control and melanoma samples. For example, in contrast to the weak upregulation in nevi, *foxd3*, *pax3a*, *sox10*, *crestin* and *zeb2a* were robustly Up in melanoma with respect to the control. On the other hand, other neural crest-related genes including *erbb2, erbb3a, erbb3b, sox9b, twist1a, twist1b and twist3* were strongly Down in melanoma while remaining Up in nevi as in control. These results suggest that NCC signature has a key role in regulation of malignant transformation of melanocytes to melanoma. For the melanocyte differentiation genes, we observed a similar pattern of regulation for nevi and melanoma. All but one of the fourteen selected genes were slightly Up in nevi and dramatically Up in melanoma as compared to the control (Figure 5A). GO term enrichment analysis displayed that nevi was mostly enriched for GO-BP terms including various types of tissue development, pigmentation and NCC signature (Figure 5B, Table S3). KEGG pathway analysis for nevi produced relatively weaker information than GO analysis and revealed several metabolic pathways as well as melanogenesis, which regulates melanin production in a specialized organelle called melanosome (Figure S3B, Table S4). On the contrary, melanoma samples were significantly enriched for the GO-BP terms related to cell proliferation, cell migration, pigmentation, development and regeneration (Figure 5C, Table S3), and for the KEGG pathways that harbored numerous cells metabolism activities and cancer-associated signaling pathways such as MAPK, p53, FoxO and ErbB (Figure S3B, Table S4). qPCR results confirmed differential expression of the genes that are regulated at either nevi or melanoma or both samples (Figure 5D, Table S1). Collectively, these data indicate that nevi and melanoma are similar with respect to induction of melanocyte differentiation and pigmentation responses and differ from each other as regard to proliferation and NCC differentiation.

Cellular processes including Wnt and BMP signaling pathways are oppositely regulated during melanocyte regeneration and melanoma

As the cellular mechanisms of regeneration and cancer display shared and distinct patterns, next we set out to compare the transcriptomes of the regenerating melanocytes to those of the nevi and melanoma. At this point, a global comparison would reveal how comparable regeneration and cancer are. Thus, by exploiting the GOChord function, we plotted a circularly composited overview of the fold changes of genes in the selected GO terms. To compare the changes in gene expression associated with these selected GO terms in the regeneration and cancer samples, we intersected the genes annotated in these terms with the DEG sets (Figure 6A). The genes obtained from the GO terms included a substantial number of genes involved in NCC migration, glial cell differentiation, fin regeneration and fin morphogenesis. Interestingly, there were groups of DEGs that are regulated oppositely between 7 dpa and melanoma and other groups of DEGs that are regulated oppositely between the two regeneration stages (1 dpa and 7 dpa) and melanoma. Similar groups of genes were present in the GOChord plots generated by using the selected KEGG pathways (Figure S4). Moreover, we unraveled the DEGs that are shared between regeneration and cancer (1 dpa-nevi, 7 dpa-nevi, 1dpa-melanoma and 7 dpa-melanoma) according to four different ways of regulation, i.e. Down-Up, Up-Up, Down-Down, Up-Down (Figure S5).

Next, we generated heatmaps of the DEGs that belong to two particular GO terms, i.e. Wnt signaling pathway and BMP signaling pathway. Strikingly, the majority of the Wnt pathway-related genes including *wnt7bb*, *wnt11r*, *wnt4a*, *wnt1*, *wnt16*, *wnt3*, *wnt6b*, *wnt7aa*, *wnt10a*, *lypd6* and *axin2* were significantly Up in 1 dpa and 7 dpa, but Down in nevi and more dramatically Down in melanoma (Figure 6B). More than half of the genes that are associated with the BMP signaling pathway including *gdf5*, *smad6a*, *grem2a*, *BMP5*, *BMP7b*, *BMP2b*, *sost*, *BMP4*, *tgfb2l*, *BMP7a* and *rgma* were likewise Down in melanoma, while not being significantly regulated or Up in 1 dpa and 7 dpa (Figure 6C). The majority of the BMP-related genes that are Up in melanoma samples were either not significantly regulated or Down in 1 dpa and 7 dpa. These results strongly suggest that Wnt and BMP signaling pathways are oppositely regulated between melanocyte regeneration and melanoma and that they promote a regenerative response, potentially also by helping the cells escape from undergoing carcinogenesis.

Activation of canonical Wnt or BMP signaling pathways enhances larval melanocyte regeneration and suppresses migration of human melanoma cells

The opposite regulation of Wnt and BMP signaling pathways between melanocyte regeneration and melanoma could propose these pathways as key mechanisms that regulate the crossroad between the two phenomena. To test this hypothesis, we aimed to manipulate the signaling pathways by using chemicals that inhibit or activate the pathway and assess the influence on the melanocytes during both regeneration and cancer. Since most of the Wnt-pathway related genes, including *wnt7bb*, *wnt1*, *wnt3*, *lypd6* and *axin2* that are regulated oppositely between melanocyte regeneration and melanoma, have been associated with the Wnt/β-catenin pathway, we decided to modify the β-catenin-dependent (canonical) Wnt signaling among the Wnt pathways (Jho, Zhang et al. 2002, Grumolato, Liu et al. 2010, Özhan, Sezgin et al. 2013, Arensman, Kovochich et al. 2014). We exploited the larval zebrafish that is rapidly responsive, easy to manipulate and permeable to small molecules.

First, to test the influence of canonical Wnt and BMP signaling pathways on melanocyte regeneration, we ablated the melanocytes of the zebrafish larvae with 4-HA from 36 hpf to 60 hpf, and treated the larvae with the Wnt antagonist IWR, Wnt agonist BIO, BMP antagonist DMH1 or BMP agonist ISL from 60 hpf to 4 dpf (Figure 7A). Upon 4-HA treatment, melanocytes were lost as early as 48 hpf (Figure 7B) and significantly reduced in number by 4 dpf (Figure 7C-D, compare DMSO to 4-HA). The inhibition of either canonical Wnt or BMP pathways further reduced their number significantly (Figure 7C-D, compare 4-HA to IWR or DMH1) while the activation of either pathway increased the number of melanocytes beyond the 4-HA level (Figure 7C-D, compare 4-HA to BIO or ISL). Second, to examine the effect of Wnt and BMP pathways on melanoma with respect to cancer cell migration and metastasis, we generated larval zebrafish xenografts by injecting DiO-labeled SK-MEL-28, a human malignant melanoma cell line, into the yolk sac at 2 dpf, treated them with the antagonists or agonists of the pathways and observed the cancer cell behavior over time. At 5 dpi, melanoma cells invaded the caudal tissue and formed micrometastasis colonies in half of the control embryos, indicating the metastatic potential of the SK-MEL-28 cells (Figure 8A-B). We observed that the inhibition of Wnt (with IWR) or BMP (with DMH1) pathway did not significantly alter cancer cell migration and the number of invading melanoma cells as compared to the control (Figure 8A-B). On the other hand, the activation of Wnt

(with BIO) or BMP (with ISL) pathway dramatically reduced their dissemination through the caudal tissue. Thus, the activation of Wnt and BMP pathways can enhance the regenerative capacities of the melanocytes and efficiently suppress the migration of melanoma cells.

Discussion

Tissue regeneration mechanisms have been discussed from the perspective of differential gene expression analysis in different tissues. However, there is limited information on the comparative analysis of the transcriptomes in different stages of regeneration and the dynamic transcriptional responses during regeneration. Recently, we have revealed the transcriptomes of the regenerating zebrafish brain at its two different stages (Demirci, Cucun et al. 2020). Here, we first extended this approach to reveal the transcriptome profiles of zebrafish melanocyte regeneration at two different stages, i.e. at 1 dpa and 7 dpa that represent the early proliferative and the late differentiation stages, respectively. Since the molecular pathways and gene expression patterns of regeneration show similarities to those of carcinogenesis, a global comparison of the transcriptomes during both phenomena could provide large amount of information on the common and distinct mechanisms of regeneration and cancer. Thus, next, by implementing this viewpoint to the melanocyte model, we generated zebrafish models of early and late melanoma and compared their transcriptomes to each other and to those of the regenerating melanocytes. We used the melanocytic nevi to represent the early stage of melanoma since a considerable percentage of all melanoma cases are associated with preexisting dysplastic moles (nevi), where MAPK-related genetic alterations are responsible for hyper-proliferation of the skin melanocytes (Bevona, Goggins et al. 2003). Thus, *kita-GFP-RAS*^{G12V} zebrafish line that develops melanocytic nevi is a valuable model to investigate the melanoma transformation from the earliest steps. To our knowledge, this is the first study that compares the molecular mechanisms of regeneration and cancer that occur within the same tissue and the same organism. Accordingly, we have reached the following conclusions: i) 1 dpa represents the proliferation stage and is used to analyze the early regeneration, while 7 dpa represents the differentiation stage and is used to examine the late regeneration at the transcriptional level. These stages significantly differ from each other with respect to the clustering and content of the DEGs. ii) While 1 dpa is enriched with DEGs related to proliferation

and cell cycle, 7 dpa is mostly characterized by DEGs associated with melanocyte differentiation and pigmentation. Genes related to immune response and NCC differentiation were generally oppositely regulated between 1 dpa and 7 dpa. iii) Samples of melanocytic nevi and malignant melanoma harbor DEGs that are substantially different from each other. Nevi was rather similar to control samples with respect to expression of selected genes related to proliferation, cell cycle and NCC differentiation, which were completely oppositely regulated in melanoma. Genes associated with melanocyte differentiation and pigmentation are weakly upregulated in nevi and strongly upregulated in melanoma. iv) Genes belonging to the Wnt and BMP signaling pathways are oppositely regulated between regeneration and cancer; i.e. majority of them are upregulated during melanocyte regeneration but downregulated in melanoma. v) During regeneration, inhibition of Wnt or BMP pathways significantly reduced the number of newly produced melanocytes while activation of either pathway increased their number. In contrast, in melanoma, the activation of Wnt or BMP pathways decreased the number of migrating melanoma cells, suggesting that these pathways operate in favor of regeneration and against cancer.

Early stage of regeneration (1dpa) and melanoma are characterized with upregulation of genes including *cdk2, mcm7, pcna, mki67* and *cdk1* that are associated with proliferation and cell cycle. On the contrary, these genes were likewise regulated between late stage of regeneration (7 dpa) and control as well as between nevi and control. These data suggest that cell proliferation is a prominent event that converges cancer to early regeneration while diverging it from late regeneration. In contrast, *cdkn1bb*, the ortholog of human *CDKN1B*, was downregulated both at 1 dpa and in melanoma. By inhibiting the activity of Cdk-cyclin complexes at the G1 phase, *CDKN1B* interferes with the G1/S transition and negatively regulates cell proliferation (Polyak, Lee et al. 1994, Sharma and Pledger 2016). Cancers carrying BRAF mutations have increased expression of cycle inhibitors including *CDKN2A*, *CDKN1A* and *CDKN1B* (Chu, Hengst et al. 2008). However, these genes have been reported to be recurrently inactivated in pre-malignant nevi with BRAF mutations and contribute to melanoma pathogenesis (Gruber, Kastelan et al. 2008, González-Ruiz, González-Moles et al. 2020). Thus, parallel downregulation of *cdkn1bb* during early melanocyte regeneration and melanoma suggests this tumor suppressor gene as a key regulator that brings early regeneration and cancer closer.

During early melanocyte regeneration, we found that, in addition to the cell cycle and proliferation genes, DNA repair signatures were significantly enriched most likely because actively proliferating cells are exposed to DNA damage more than any other tissue. Strikingly, even though early melanocyte regeneration and melanoma are similar with respect to enrichment of genes related to cell proliferation, they look completely different with respect to the activation of DNA repair mechanisms. Whereas early regeneration was enriched for various types of DNA repair including base excision, mismatch and double strand break, melanoma showed no enrichment for DNA repair pathways. This is also supported by enrichment of the KEGG pathway called Fanconi anemia that has been shown to promote homologous recombination upon DNA interstrand crosslinks by suppressing nucleotide-excision repair and is mostly deregulated in cancer predispositions (Sancar and Tang 1993, Michl, Zimmer et al. 2016, Fang, Wu et al. 2020, Zhang, Mou et al. 2021). Proper activation of DNA repair mechanisms is essential for homeostatic renewal and tissue regeneration following injury since defects in these mechanisms could interfere with the ability of adult stem cells to rebuild healthy tissues and increase the susceptibility of malignant transformations (Al Zouabi and Bardin 2020). Thus, while maintaining an exquisite balance between proliferation and differentiation, tissue regeneration carries the risk of malignant transformations once the cells escape from the rigid control of cell cycle and DNA repair mechanisms, especially at the early stages of regeneration.

In contrast to the modest increase in expression of NCC signature in nevi, melanoma showed a dramatic increase in NCC genes including *foxd3*, *pax3a*, *sox10*, *crestin* and *zeb2a*. Upregulation of *crestin* is in line with its instant re-expression at the onset of melanoma (Kaufman, Mosimann et al. 2016, McConnell, Mito et al. 2019). On the other hand, *foxd3* acts as a repressor of *mitfa* and inhibits melanocyte differentiation during NCC development (Curran, Lister et al. 2010). Therefore, elevated *foxd3* expression in our melanoma samples could be related to the increase in stemness/less differentiated phenotype. The transcriptome profile of our nevi samples appear to rather resemble that of the superficial spreading melanoma, where the stem cell-related genes *erbb2* and *erbb3* and the mesenchymal signatures *sox9*, *twist1a*, *twist1b* and *twist3* showed increased expression (Buac, Xu et al. 2009, Travnickova, Wojciechowska et al. 2019).

One of the most prominent effects shared between late melanocyte regeneration and melanoma is the evident upregulation of genes involved in melanocyte differentiation and pigmentation. One of those genes, the *mitfa* gene that is essential for the development of melanocytes, has been reported to have contradictory roles in melanoma. For example, *MITF* amplification is found in 15- 20% of human metastatic melanomas with poor prognosis (Ugurel, Houben et al. 2007). MITF has been shown to directly regulate a set of genes required for cell proliferation and DNA repair and thus inhibit cellular senescence (Strub, Giuliano et al. 2011). Moreover, MITF was found to be expressed at high levels in melanomas resistant to chemotherapeutic agents as well as in melanoma relapse after targeted therapy against BRAF mutations and MEK activity (Garraway, Widlund et al. 2005, Van Allen, Wagle et al. 2014). On the contrary, *mitf* expression at lower levels has also been associated with resistance to targeted therapy and increased invasiveness of melanomas (Javelaud, Alexaki et al. 2011, Eccles, He et al. 2013, Müller, Krijgsman et al. 2014). These paradoxical functions of MITF to both promote and inhibit proliferation of melanoma cells has been explained by the "MITF rheostat" model, where its high-level, mid-level, low-level and absence promote differentiation, proliferation, invasion and cell death, respectively (Carreira, Goodall et al. 2006, Hoek and Goding 2010, Seberg, Van Otterloo et al. 2017). Thus, increased expression of *mitfa* in our melanoma samples is likely associated with survival and proliferation of tumor cells as the samples were at the same time significantly enriched for the cell cycle and proliferation-related signatures. The key role of human *MITF* in melanocyte differentiation occurs through direct transcriptional control of several genes including TYR, TYRP1, DCT, KIT, MC1R, PMEL17 and SLC45A2 as well as indirect ones such as EDNRB (Sato-Jin, Nishimura et al. 2008, Cheli, Ohanna et al. 2010). We have found an array of pigmentation genes including *kita*, *dct*, *tyrp1a*, *tyrp1b*, *ednrba*, *ednrbb*, *mc1r*, *pmela* and *slc45a2* to be significantly upregulated during late melanocyte regeneration and melanoma, strongly suggesting that their expression is transcriptionally controlled by *mitfa*. At this point, it is important to mention that we found *Tg(mitfa+/-;kita-GFP-RAS^{G12V})* zebrafish to develop tissues of amelanotic melanoma, a subtype of melanoma that has little to no pigment, which express relatively lower levels of *mitfa* than the pigmented melanoma tissue (data not shown). The human amelanotic melanoma A375 cells were also reported to express a very low level

of *MITF* and its target gene *TYR* (Beuret, Flori et al. 2007). Therefore, it is likely that the level of *mitfa* is key to adjust the target gene expression and determine the subtype of melanoma.

Our data suggest that regenerating tissue and tumor mass diverge with respect to regulation of Wnt and BMP signaling pathways, especially in the late stages of regeneration and cancer. As both pathways showed a general tendency to be upregulated in melanocyte regeneration and downregulation in melanoma, it would be interesting to test whether they are necessary for regeneration and able to interfere with the malignant behavior of the cancer cells. Our functional analysis in the zebrafish larvae indeed showed that the activation of canonical Wnt or BMP pathways was essential for efficient melanocyte regeneration while their inhibition impaired the regenerative potential of melanocytes upon ablation. On the other hand, the activation of Wnt or BMP signaling has the ability to strongly suppress the migration of human melanoma cells in the zebrafish xenograft model. The early activation of the Wnt pathway during melanocyte regeneration is in line with our previous data that have shown active canonical Wnt signaling in the regenerating zebrafish brain at approximately 1 day post-injury (Demirci, Cucun et al. 2020). Our results have further supported the findings obtained from the loss-of-function mouse models, which dissected the collaborative role of Wnt and BMP signaling pathways in triggering the commitment of proliferative MSCs to differentiation in an MITF-dependent manner (Infarinato, Stewart et al. 2020). In addition to activating Wnt signaling, GSK3 inhibitor BIO treatment has been shown to promote nuclear localization of MITF in SK-MEL-28 cells (Ngeow, Friedrichsen et al. 2018). Our findings are consistent with this scenario since canonical Wnt signaling concomitantly increased β-catenin mediated MITF expression and stability (Takeda, Yasumoto et al. 2000, Ploper, Taelman et al. 2015). This brings us back to the rheostat role of MITF in melanoma, where high MITF activity is associated to proliferation and differentiation whereas low MITF activity is related to stem cell-like and invasive phenotype and correlated with the decreased migratory behavior of SK-MEL-28 cells upon BIO treatment. Therefore, these regeneration-promoting and cancer-suppressing roles of canonical Wnt and BMP signaling pathways can be exploited to stop tumor growth and metastasis by directing tumor cells into a regeneration-like route.

In conclusion, we took advantage of modeling melanocyte regeneration and melanoma in zebrafish that can efficiently regenerate and be induced to form cancers in zebrafish, enabling regeneration and cancer

to be successfully modeled and compared within the same organism. Moreover, by restricting the tissue for sample collection to the same organ, i.e. the caudal fin, which harbors melanocytes to efficiently model melanocyte regeneration and melanoma, we aimed to minimize the differences that might stem from the source tissue. Our detailed transcriptome analyses have revealed the common and distinct genes and pathways between melanocyte regeneration and melanoma at their early and late stages. Characterization of those pathways that secure proper initiation and termination of the proliferation and differentiation states during regeneration could be remarkably useful to inhibit tumor growth. Thus, it might be possible to interfere with cancer progression by modifying the gene expression programs of cancer cells to those of regenerating cells so that cancer cells would be able to cease abnormal growth and regain control over the cellular events, terminate growth and potentially 'achieve to heal'.

Data Availability

All datasets have been deposited in ArrayExpress under the link: https://www.ebi.ac.uk/arrayexpress/experiments/E-MTAB-11163/ with the accession number "E-MTAB-11163".

Acknowledgement

We would like to thank Dr. Adam Hurlstone for the zebrafish lines *mitfa*-/- (*nacre*) and *kita*:GFP-RAS^{G12V}. We would like to thank Izmir Biomedicine and Genome Center Vivarium-Zebrafish Core Facility, Optical Imaging Core Facility and Histopathology Core Facility for providing zebrafish care, microscope facility support and histopathology service support, respectively. We also thank the Genomics Core Facility (GeneCore) of EMBL, Heidelberg.

Ethics Statement

The animal study was reviewed and approved by the Animal Experiments Local Ethics Committee of Izmir Biomedicine and Genome Center (IBG-AELEC).

Funding

This work was supported by the Scientific and Technological Research Council of Turkey (TUBITAK, grant number 219Z040). GO Lab is funded by EMBO Installation Grant (IG 3024). EK and YD were supported by TUBITAK 2211-C Domestic Priority Areas Doctoral Scholarship Program. YD was supported by a TUBITAK 2214-A International Research Fellowship Program for PhD Students.

Author Contributions

GO and EK designed the experiments. EK performed the molecular and cell biology experiments. YD and GH conducted the bioinformatics analyses. GO and EK wrote the manuscript. All authors contributed to the discussion.

Conflict of Interest

The authors declare that they have no conflict of interest.

References

Agata, K. and K. Watanabe (1999). "Molecular and cellular aspects of planarian regeneration." Semin Cell Dev Biol **10**(4): 377-383.

Akyilmaz, E., E. Yorganci and E. Asav (2010). "Do copper ions activate tyrosinase enzyme? A biosensor model for the solution." Bioelectrochemistry **78**(2): 155-160.

Al Zouabi, L. and A. J. Bardin (2020). "Stem Cell DNA Damage and Genome Mutation in the Context of Aging and Cancer Initiation." Cold Spring Harb Perspect Biol **12**(10).

Andrews, S. (2010). A quality control tool for high throughput sequence data.

Arensman, M. D., A. N. Kovochich, R. M. Kulikauskas, A. R. Lay, P. T. Yang, X. Li, T. Donahue, M. B. Major, R. T. Moon, A. J. Chien and D. W. Dawson (2014). "WNT7B mediates autocrine Wnt/β-catenin signaling and anchorage-independent growth in pancreatic adenocarcinoma." Oncogene **33**(7): 899-908.

Beachy, P. A., S. S. Karhadkar and D. M. Berman (2004). "Tissue repair and stem cell renewal in carcinogenesis." Nature **432**(7015): 324-331.

Beuret, L., E. Flori, C. Denoyelle, K. Bille, R. Busca, M. Picardo, C. Bertolotto and R. Ballotti (2007). "Up-regulation of MET expression by alpha-melanocyte-stimulating hormone and MITF allows hepatocyte growth factor to protect melanocytes and melanoma cells from apoptosis." J Biol Chem **282**(19): 14140-14147.

Bevona, C., W. Goggins, T. Quinn, J. Fullerton and H. Tsao (2003). "Cutaneous melanomas associated with nevi." Arch Dermatol **139**(12): 1620-1624; discussion 1624.

Brockes, J. P. and A. Kumar (2008). "Comparative aspects of animal regeneration." Annu Rev Cell Dev Biol **24**: 525-549.

Buac, K., M. Xu, J. Cronin, A. T. Weeraratna, S. M. Hewitt and W. J. Pavan (2009). "NRG1 / ERBB3 signaling in melanocyte development and melanoma: inhibition of differentiation and promotion of proliferation." Pigment Cell Melanoma Res **22**(6): 773-784.

Cajal, S. R. (1928). Degeneration and regeneration in the nervous system. London, Oxford University Press.

Carreira, S., J. Goodall, L. Denat, M. Rodriguez, P. Nuciforo, K. S. Hoek, A. Testori, L. Larue and C. R. Goding (2006). "Mitf regulation of Dia1 controls melanoma proliferation and invasiveness." Genes Dev **20**(24): 3426-3439.

Ceol, C. J., Y. Houvras, R. M. White and L. I. Zon (2008). "Melanoma biology and the promise of zebrafish." Zebrafish **5**(4): 247-255.

Cheli, Y., M. Ohanna, R. Ballotti and C. Bertolotto (2010). "Fifteen-year quest for microphthalmia-associated transcription factor target genes." Pigment Cell Melanoma Res **23**(1): 27-40.

Chu, I. M., L. Hengst and J. M. Slingerland (2008). "The Cdk inhibitor p27 in human cancer: prognostic potential and relevance to anticancer therapy." Nat Rev Cancer **8**(4): 253-267.

Cichorek, M., M. Wachulska, A. Stasiewicz and A. Tyminska (2013). "Skin melanocytes: biology and development." Postepy Dermatol Alergol **30**(1): 30-41.

Coussens, L. M. and Z. Werb (2002). "Inflammation and cancer." Nature **420**(6917): 860-867.

Crusz, S. M. and F. R. Balkwill (2015). "Inflammation and cancer: advances and new agents." Nat Rev Clin Oncol **12**(10): 584-596.

Curado, S., R. M. Anderson, B. Jungblut, J. Mumm, E. Schroeter and D. Y. Stainier (2007). "Conditional targeted cell ablation in zebrafish: a new tool for regeneration studies." Dev Dyn **236**(4): 1025-1035.

Curran, K., J. A. Lister, G. R. Kunkel, A. Prendergast, D. M. Parichy and D. W. Raible (2010). "Interplay between Foxd3 and Mitf regulates cell fate plasticity in the zebrafish neural crest." Dev Biol **344**(1): 107-118.

Demirci, Y., G. Cucun, Y. K. Poyraz, S. Mohammed, G. Heger, I. Papatheodorou and G. Ozhan (2020). "Comparative Transcriptome Analysis of the Regenerating Zebrafish Telencephalon Unravels a Resource With Key Pathways During Two Early Stages and Activation of Wnt/beta-Catenin Signaling at the Early Wound Healing Stage." Front Cell Dev Biol **8**: 584604.

DiPietro, L. A. (2013). "Angiogenesis and scar formation in healing wounds." Curr Opin Rheumatol **25**(1): 87-91.

DiPietro, L. A. (2016). "Angiogenesis and wound repair: when enough is enough." J Leukoc Biol.

Dolberg, D. S., R. Hollingsworth, M. Hertle and M. J. Bissell (1985). "Wounding and its role in RSV-mediated tumor formation." Science **230**(4726): 676-678.

Dvorak, H. F. (2015). "Tumors: wounds that do not heal-redux." Cancer Immunol Res **3**(1): 1-11.

Eccles, M. R., S. He, A. Ahn, L. J. Slobbe, A. R. Jeffs, H. S. Yoon and B. C. Baguley (2013). "MITF and PAX3 Play Distinct Roles in Melanoma Cell Migration; Outline of a "Genetic Switch" Theory Involving MITF and PAX3 in Proliferative and Invasive Phenotypes of Melanoma." Front Oncol **3**: 229.

Eming, S. A., P. Martin and M. Tomic-Canic (2014). "Wound repair and regeneration: mechanisms, signaling, and translation." Sci Transl Med **6**(265): 265sr266.

Fang, C. B., H. T. Wu, M. L. Zhang, J. Liu and G. J. Zhang (2020). "Fanconi Anemia Pathway: Mechanisms of Breast Cancer Predisposition Development and Potential Therapeutic Targets." Front Cell Dev Biol **8**: 160.

Forbes, S. A., D. Beare, H. Boutselakis, S. Bamford, N. Bindal, J. Tate, C. G. Cole, S. Ward, E. Dawson, L. Ponting, R. Stefancsik, B. Harsha, C. Y. Kok, M. Jia, H. Jubb, Z. Sondka, S. Thompson, T. De and P. J. Campbell (2017). "COSMIC: somatic cancer genetics at high-resolution." Nucleic Acids Res **45**(D1): D777-d783.

Foster, J. A. (1963). "Induction of neoplasms in planarians with carcinogens." Cancer Res **23**: 300-303.

Fountain, J. W., M. Karayiorgou, M. S. Ernstoff, J. M. Kirkwood, D. R. Vlock, L. Titus-Ernstoff, B. Bouchard, S. Vijayasaradhi, A. N. Houghton, J. Lahti and et al. (1992). "Homozygous deletions within human chromosome band 9p21 in melanoma." Proc Natl Acad Sci U S A **89**(21): 10557-10561.

Garbe, C., K. Peris, A. Hauschild, P. Saiag, M. Middleton, L. Bastholt, J. J. Grob, J. Malvehy, J. Newton-Bishop, A. J. Stratigos, H. Pehamberger and A. M. Eggermont (2016). "Diagnosis and treatment of melanoma. European consensus-based interdisciplinary guideline - Update 2016." Eur J Cancer **63**: 201-217.

Garraway, L. A., H. R. Widlund, M. A. Rubin, G. Getz, A. J. Berger, S. Ramaswamy, R. Beroukhim, D. A. Milner, S. R. Granter, J. Du, C. Lee, S. N. Wagner, C. Li, T. R. Golub, D. L. Rimm, M. L. Meyerson, D. E. Fisher and W. R. Sellers (2005). "Integrative genomic analyses identify MITF as a lineage survival oncogene amplified in malignant melanoma." Nature **436**(7047): 117-122.

González-Ruiz, L., M. González-Moles, I. González-Ruiz, I. Ruiz-Ávila, Á. Ayén and P. Ramos-García (2020). "An update on the implications of cyclin D1 in melanomas." Pigment Cell Melanoma Res **33**(6): 788-805.

Gruber, F., M. Kastelan, I. Brajac, M. Saftić, V. Peharda, L. Cabrijan, Z. Stanić Zgombić and E. Simonić (2008). "Molecular and genetic mechanisms in melanoma." Coll Antropol **32 Suppl 2**: 147-152.

Grumolato, L., G. Liu, P. Mong, R. Mudbhary, R. Biswas, R. Arroyave, S. Vijayakumar, A. N. Economides and S. A. Aaronson (2010). "Canonical and noncanonical Wnts use a common mechanism to activate completely unrelated coreceptors." Genes Dev **24**(22): 2517-2530.

Guo, H., Y. Xing, Y. Liu, Y. Luo, F. Deng, T. Yang, K. Yang and Y. Li (2016). "Wnt/beta-catenin signaling pathway activates melanocyte stem cells in vitro and in vivo." J Dermatol Sci **83**(1): 45-51.

Gurtner, G. C., S. Werner, Y. Barrandon and M. T. Longaker (2008). "Wound repair and regeneration." Nature **453**(7193): 314-321.

Haddow, A. (1972). "Molecular repair, wound healing, and carcinogenesis: tumor production a possible overhealing?" Adv Cancer Res **16**: 181-234.

Hall, F., M. Morita and J. B. Best (1986). "Neoplastic transformation in the planarian: II. Ultrastructure of malignant reticuloma." J Exp Zool **240**(2): 229-244.

Higdon, C. W., R. D. Mitra and S. L. Johnson (2013). "Gene expression analysis of zebrafish melanocytes, iridophores, and retinal pigmented epithelium reveals indicators of biological function and developmental origin." PLoS One **8**(7): e67801.

Hoek, K. S. and C. R. Goding (2010). "Cancer stem cells versus phenotype-switching in melanoma." Pigment Cell Melanoma Res **23**(6): 746-759.

Huang da, W., B. T. Sherman and R. A. Lempicki (2009). "Systematic and integrative analysis of large gene lists using DAVID bioinformatics resources." Nat Protoc **4**(1): 44-57.

Infarinato, N. R., K. S. Stewart, Y. Yang, N. C. Gomez, H. A. Pasolli, L. Hidalgo, L. Polak, T. S. Carroll and E. Fuchs (2020). "BMP signaling: at the gate between activated melanocyte stem cells and differentiation." Genes Dev **34**(23-24): 1713-1734.

Iyengar, S., M. Kasheta and C. J. Ceol (2015). "Poised Regeneration of Zebrafish Melanocytes Involves Direct Differentiation and Concurrent Replenishment of Tissue-Resident Progenitor Cells." Dev Cell **33**(6): 631-643.

Javelaud, D., V. I. Alexaki, M. J. Pierrat, K. S. Hoek, S. Dennler, L. Van Kempen, C. Bertolotto, R. Ballotti, S. Saule, V. Delmas and A. Mauviel (2011). "GLI2 and M-MITF transcription factors control exclusive gene expression programs and inversely regulate invasion in human melanoma cells." Pigment Cell Melanoma Res **24**(5): 932-943.

Jho, E. H., T. Zhang, C. Domon, C. K. Joo, J. N. Freund and F. Costantini (2002). "Wnt/beta-catenin/Tcf signaling induces the transcription of Axin2, a negative regulator of the signaling pathway." Mol Cell Biol **22**(4): 1172-1183.

Kang, J., R. Karra and K. D. Poss (2015). "Back in Black." Dev Cell **33**(6): 623-624.

Karin, M. and H. Clevers (2016). "Reparative inflammation takes charge of tissue regeneration." Nature **529**(7586): 307-315.

Kaufman, C. K., C. Mosimann, Z. P. Fan, S. Yang, A. J. Thomas, J. Ablain, J. L. Tan, R. D. Fogley, E. van Rooijen, E. J. Hagedorn, C. Ciarlo, R. M. White, D. A. Matos, A. C. Puller, C. Santoriello, E. C. Liao, R. A. Young and L. I. Zon (2016). "A zebrafish melanoma model reveals emergence of neural crest identity during melanoma initiation." Science **351**(6272): aad2197.

Kim, D., B. Langmead and S. L. Salzberg (2015). "HISAT: a fast spliced aligner with low memory requirements." Nat Methods **12**(4): 357-360.

King, R. S. and P. A. Newmark (2012). "The cell biology of regeneration." J Cell Biol **196**(5): 553-562.

Kolde, R. (2012). "Pheatmap: pretty heatmaps." R package version **1**(2): 726.

Krauss, J., H. G. Frohnhöfer, B. Walderich, H.-M. Maischein, C. Weiler, U. Irion and C. Nüsslein-Volhard (2014). "Endothelin signalling in iridophore development and stripe pattern formation of zebrafish." Biology open **3**(6): 503-509.

Kumano, K., S. Masuda, M. Sata, T. Saito, S. Y. Lee, M. Sakata-Yanagimoto, T. Tomita, T. Iwatsubo, H. Natsugari, M. Kurokawa, S. Ogawa and S. Chiba (2008). "Both Notch1 and Notch2 contribute to the regulation of melanocyte homeostasis." Pigment Cell Melanoma Res **21**(1): 70-78.

Lin, S. J., M. C. Chiang, H. Y. Shih, L. S. Hsu, T. H. Yeh, Y. C. Huang, C. Y. Lin and Y. C. Cheng (2017). "Regulator of G protein signaling 2 (Rgs2) regulates neural crest development through Pparδ-Sox10 cascade." Biochim Biophys Acta Mol Cell Res **1864**(3): 463-474.

Lister, J. A., C. P. Robertson, T. Lepage, S. L. Johnson and D. W. Raible (1999). "nacre encodes a zebrafish microphthalmia-related protein that regulates neural-crest-derived pigment cell fate." Development **126**(17): 3757-3767.

Liu, J., M. Fukunaga-Kalabis, L. Li and M. Herlyn (2014). "Developmental pathways activated in melanocytes and melanoma." Arch Biochem Biophys **563**: 13-21.

Love, M. I., W. Huber and S. Anders (2014). "Moderated estimation of fold change and dispersion for RNA-seq data with DESeq2." Genome Biol **15**(12): 550.

MacCarthy-Morrogh, L. and P. Martin (2020). "The hallmarks of cancer are also the hallmarks of wound healing." Sci Signal **13**(648).

Martinez-Lopez, M., V. Póvoa and R. Fior (2021). "Generation of Zebrafish Larval Xenografts and Tumor Behavior Analysis." J Vis Exp(172).

McConnell, A. M., J. K. Mito, J. Ablain, M. Dang, L. Formichella, D. E. Fisher and L. I. Zon (2019). "Neural crest state activation in NRAS driven melanoma, but not in NRAS-driven melanocyte expansion." Dev Biol **449**(2): 107-114.

McGill, G. G., M. Horstmann, H. R. Widlund, J. Du, G. Motyckova, E. K. Nishimura, Y. L. Lin, S. Ramaswamy, W. Avery, H. F. Ding, S. A. Jordan, I. J. Jackson, S. J. Korsmeyer, T. R. Golub and D. E. Fisher (2002). "Bcl2 regulation by the melanocyte master regulator Mitf modulates lineage survival and melanoma cell viability." Cell **109**(6): 707-718.

Michl, J., J. Zimmer and M. Tarsounas (2016). "Interplay between Fanconi anemia and homologous recombination pathways in genome integrity." Embo j **35**(9): 909-923.

Mort, R. L., I. J. Jackson and E. E. Patton (2015). "The melanocyte lineage in development and disease." Development **142**(4): 620-632.

Müller, J., O. Krijgsman, J. Tsoi, L. Robert, W. Hugo, C. Song, X. Kong, P. A. Possik, P. D. Cornelissen-Steijger, M. H. Geukes Foppen, K. Kemper, C. R. Goding, U. McDermott, C. Blank, J. Haanen, T. G. Graeber, A. Ribas, R. S. Lo and D. S. Peeper (2014). "Low MITF/AXL ratio predicts early resistance to multiple targeted drugs in melanoma." Nat Commun **5**: 5712.

Ngeow, K. C., H. J. Friedrichsen, L. Li, Z. Zeng, S. Andrews, L. Volpon, H. Brunsdon, G. Berridge, S. Picaud, R. Fischer, R. Lisle, S. Knapp, P. Filippakopoulos, H. Knowles, E. Steingrímsson, K. L. B. Borden, E. E. Patton and C. R. Goding (2018). "BRAF/MAPK and GSK3 signaling converges to control MITF nuclear export." Proc Natl Acad Sci U S A **115**(37): E8668-e8677.

Nishimura, E. K., S. A. Jordan, H. Oshima, H. Yoshida, M. Osawa, M. Moriyama, I. J. Jackson, Y. Barrandon, Y. Miyachi and S. Nishikawa (2002). "Dominant role of the niche in melanocyte stem-cell fate determination." Nature **416**(6883): 854-860.

O'Reilly-Pol, T. and S. L. Johnson (2008). "Neocuproine ablates melanocytes in adult zebrafish." Zebrafish **5**(4): 257-264.

O'Reilly-Pol, T. and S. L. Johnson (2013). "Kit signaling is involved in melanocyte stem cell fate decisions in zebrafish embryos." Development **140**(5): 996-1002.

Oshima, H., A. Rochat, C. Kedzia, K. Kobayashi and Y. Barrandon (2001). "Morphogenesis and renewal of hair follicles from adult multipotent stem cells." Cell **104**(2): 233-245.

Oviedo, N. J. and W. S. Beane (2009). "Regeneration: The origin of cancer or a possible cure?" Semin Cell Dev Biol **20**(5): 557-564.

Özhan, G., E. Sezgin, D. Wehner, A. S. Pfister, S. J. Kühl, B. Kagermeier-Schenk, M. Kühl, P. Schwille and G. Weidinger (2013). "Lypd6 enhances Wnt/β-catenin signaling by promoting Lrp6 phosphorylation in raft plasma membrane domains." Dev Cell **26**(4): 331-345.

Plonka, P. M., T. Passeron, M. Brenner, D. J. Tobin, S. Shibahara, A. Thomas, A. Slominski, A. L. Kadekaro, D. Hershkovitz, E. Peters, J. J. Nordlund, Z. Abdel-Malek, K. Takeda, R. Paus, J. P. Ortonne, V. J. Hearing and K. U. Schallreuter (2009). "What are melanocytes really doing all day long...?" Exp Dermatol **18**(9): 799-819.

Ploper, D., V. F. Taelman, L. Robert, B. S. Perez, B. Titz, H. W. Chen, T. G. Graeber, E. von Euw, A. Ribas and E. M. De Robertis (2015). "MITF drives endolysosomal biogenesis and potentiates Wnt signaling in melanoma cells." Proc Natl Acad Sci U S A **112**(5): E420-429.

Polyak, K., M. H. Lee, H. Erdjument-Bromage, A. Koff, J. M. Roberts, P. Tempst and J. Massagué (1994). "Cloning of p27Kip1, a cyclin-dependent kinase inhibitor and a potential mediator of extracellular antimitogenic signals." Cell **78**(1): 59-66.

Rawls, J. F. and S. L. Johnson (2001). "Requirements for the kit receptor tyrosine kinase during regeneration of zebrafish fin melanocytes." Development **128**(11): 1943-1949.

Riss, J., C. Khanna, S. Koo, G. V. Chandramouli, H. H. Yang, Y. Hu, D. E. Kleiner, A. Rosenwald, C. F. Schaefer, S. A. Ben-Sasson, L. Yang, J. Powell, D. W. Kane, R. A. Star, O. Aprelikova, K. Bauer, J. R. Vasselli, J. K. Maranchie, K. W. Kohn, K. H. Buetow, W. M. Linehan, J. N. Weinstein, M. P. Lee, R. D. Klausner and J. C. Barrett (2006). "Cancers as wounds that do not heal: differences and similarities between renal regeneration/repair and renal cell carcinoma." Cancer Res **66**(14): 7216-7224.

Rose, S. M. and F. C. Rose (1952). "Tumor agent transformations in Amphibia." Cancer Res **12**(1): 1-12.

Rose, S. M. and H. M. Wallingford (1948). "Transformation of renal tumors of frogs to normal tissues in regenerating limbs of salamanders." Science **107**(2784): 457.

Sancar, A. and M.-s. Tang (1993). "NUCLEOTIDE EXCISION REPAIR." Photochemistry and Photobiology **57**(5): 905-921.

Sanchez Alvarado, A. and P. A. Tsonis (2006). "Bridging the regeneration gap: genetic insights from diverse animal models." Nat Rev Genet **7**(11): 873-884.

Santoriello, C., E. Gennaro, V. Anelli, M. Distel, A. Kelly, R. W. Koster, A. Hurlstone and M. Mione (2010). "Kita driven expression of oncogenic HRAS leads to early onset and highly penetrant melanoma in zebrafish." PLoS One **5**(12): e15170.

Sato-Jin, K., E. K. Nishimura, E. Akasaka, W. Huber, H. Nakano, A. Miller, J. Du, M. Wu, K. Hanada, D. Sawamura, D. E. Fisher and G. Imokawa (2008). "Epistatic connections between microphthalmia-associated transcription factor and endothelin signaling in Waardenburg syndrome and other pigmentary disorders." Faseb j **22**(4): 1155-1168.

Schafer, M. and S. Werner (2008). "Cancer as an overhealing wound: an old hypothesis revisited." Nat Rev Mol Cell Biol **9**(8): 628-638.

Schmidt, E. E., K. Ichimura, K. R. Messerle, H. M. Goike and V. P. Collins (1997). "Infrequent methylation of CDKN2A(MTS1/p16) and rare mutation of both CDKN2A and CDKN2B(MTS2/p15) in primary astrocytic tumours." Br J Cancer **75**(1): 2-8.

Seberg, H. E., E. Van Otterloo and R. A. Cornell (2017). "Beyond MITF: Multiple transcription factors directly regulate the cellular phenotype in melanocytes and melanoma." Pigment Cell Melanoma Res **30**(5): 454-466.

Seilern-Aspang, F. and K. Kratochwill (1962). "Induction and differentiation of an epithelial tumour in the newt (Triturus cristatus)." J Embryol Exp Morphol **10**: 337-356.

Serrano, M., G. J. Hannon and D. Beach (1993). "A new regulatory motif in cell-cycle control causing specific inhibition of cyclin D/CDK4." Nature **366**(6456): 704-707.

Sharma, S. S. and W. J. Pledger (2016). "The non-canonical functions of p27(Kip1) in normal and tumor biology." Cell Cycle **15**(9): 1189-1201.

Silva, N. J., M. Nagashima, J. Li, L. Kakuk-Atkins, M. Ashrafzadeh, D. R. Hyde and P. F. Hitchcock (2020). "Inflammation and matrix metalloproteinase 9 (Mmp-9) regulate photoreceptor regeneration in adult zebrafish." Glia **68**(7): 1445-1465.

Stern, C. D. (2000). "Conrad H. Waddington's contributions to avian and mammalian development, 1930-1940." Int J Dev Biol **44**(1): 15-22.

Strub, T., S. Giuliano, T. Ye, C. Bonet, C. Keime, D. Kobi, S. Le Gras, M. Cormont, R. Ballotti, C. Bertolotto and I. Davidson (2011). "Essential role of microphthalmia transcription factor for DNA replication, mitosis and genomic stability in melanoma." Oncogene **30**(20): 2319-2332.

Sulaimon, S. S. and B. E. Kitchell (2003). "The biology of melanocytes." Vet Dermatol **14**(2): 57-65.

Takeda, K., N. H. Takahashi and S. Shibahara (2007). "Neuroendocrine functions of melanocytes: beyond the skin-deep melanin maker." Tohoku J Exp Med **211**(3): 201-221.

Takeda, K., K. Yasumoto, R. Takada, S. Takada, K. Watanabe, T. Udono, H. Saito, K. Takahashi and S. Shibahara (2000). "Induction of melanocyte-specific microphthalmia-associated transcription factor by Wnt-3a." J Biol Chem **275**(19): 14013-14016.

Takeo, M., W. Lee, P. Rabbani, Q. Sun, H. Hu, C. H. Lim, P. Manga and M. Ito (2016). "EdnrB Governs Regenerative Response of Melanocyte Stem Cells by Crosstalk with Wnt Signaling." Cell Rep **15**(6): 1291-1302.

Travnickova, J., S. Wojciechowska, A. Khamseh, P. Gautier, D. V. Brown, T. Lefevre, A. Brombin, A. Ewing, A. Capper, M. Spitzer, R. Dilshat, C. A. Semple, M. E. Mathers, J. A. Lister, E. Steingrimsson, T. Voet, C. P. Ponting and E. E. Patton (2019). "Zebrafish MITF-Low Melanoma Subtype Models Reveal Transcriptional Subclusters and MITF-Independent Residual Disease." Cancer Res **79**(22): 5769-5784.

Tsonis, P. A. (1983). "Effects of carcinogens on regenerating and non-regenerating limbs in amphibia (review)." Anticancer Res **3**(3): 195-202.

Ugurel, S., R. Houben, D. Schrama, H. Voigt, M. Zapatka, D. Schadendorf, E. B. Bröcker and J. C. Becker (2007). "Microphthalmia-associated transcription factor gene amplification in metastatic melanoma is a prognostic marker for patient survival, but not a predictive marker for chemosensitivity and chemotherapy response." Clin Cancer Res **13**(21): 6344-6350.

Van Allen, E. M., N. Wagle, A. Sucker, D. J. Treacy, C. M. Johannessen, E. M. Goetz, C. S. Place, A. Taylor-Weiner, S. Whittaker, G. V. Kryukov, E. Hodis, M. Rosenberg, A. McKenna, K. Cibulskis, D. Farlow, L. Zimmer, U. Hillen, R. Gutzmer, S. M. Goldinger, S. Ugurel, H. J. Gogas, F. Egberts, C. Berking, U. Trefzer, C. Loquai, B. Weide, J. C. Hassel, S. B. Gabriel, S. L. Carter, G. Getz, L. A. Garraway and D. Schadendorf (2014). "The genetic landscape of clinical resistance to RAF inhibition in metastatic melanoma." Cancer Discov **4**(1): 94-109.

Waddington , C. H. (1935). "Cancer and the Theory of Organisers." Nature **135**: 606-608.

Walter, W., F. Sanchez-Cabo and M. Ricote (2015). "GOplot: an R package for visually combining expression data with functional analysis." Bioinformatics **31**(17): 2912-2914.

Wang, X. P., Y. L. Liu, L. Y. Mei, C. F. He, Z. J. Niu, J. Sun, Y. L. Zhao, Y. Feng and H. Zhang (2018). "Wnt signaling pathway involvement in genotypic and phenotypic variations in Waardenburg syndrome type 2 with MITF mutations." J Hum Genet **63**(5): 639-646.

Watanabe, N., T. Motohashi, M. Nishioka, N. Kawamura, T. Hirobe and T. Kunisada (2016). "Multipotency of melanoblasts isolated from murine skin depends on the Notch signal." Dev Dyn **245**(4): 460-471.

White, R. M. and L. I. Zon (2008). "Melanocytes in development, regeneration, and cancer." Cell Stem Cell **3**(3): 242-252.

Wickham, H. (2016). Ggplot2: Elegant Graphics for Data Analysis. New York, Springer-Verlag.

Widlund, H. R. and D. E. Fisher (2003). "Microphthalamia-associated transcription factor: a critical regulator of pigment cell development and survival." Oncogene **22**(20): 3035-3041.

Yang, C. T. and S. L. Johnson (2006). "Small molecule-induced ablation and subsequent regeneration of larval zebrafish melanocytes." Development **133**(18): 3563-3573.

Yeh, I. and B. C. Bastian (2021). "Melanoma pathology: new approaches and classification." Br J Dermatol **185**(2): 282-293.

Zhang, J., Y. Mou, H. Gong, H. Chen and H. Xiao (2021). "Microphthalmia-Associated Transcription Factor in Senescence and Age-Related Diseases." Gerontology **67**(6): 708-717.

Figures

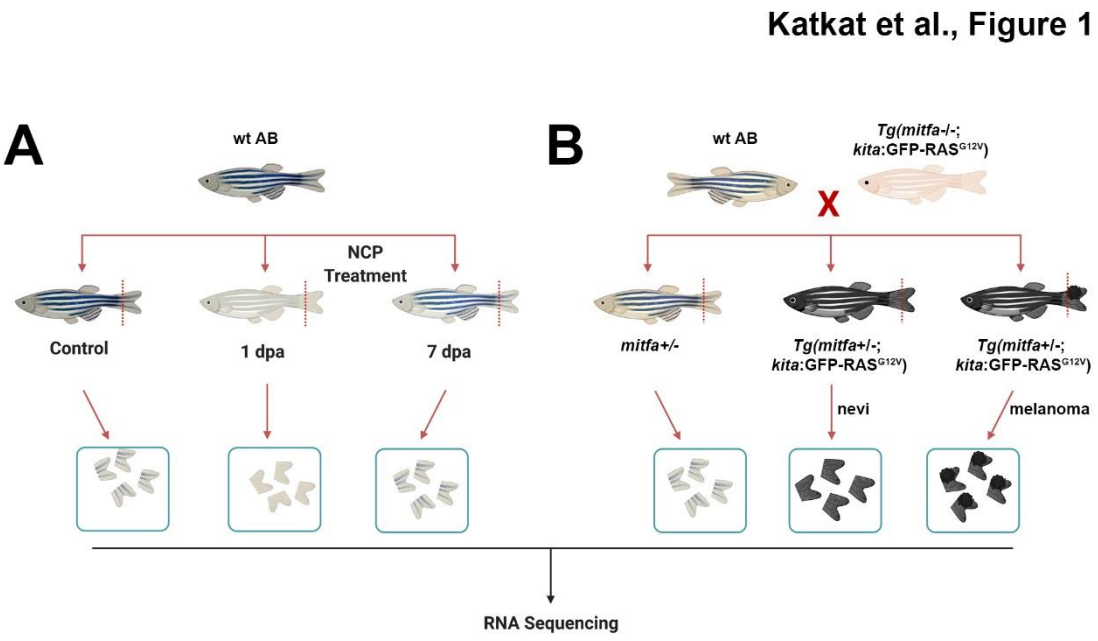

Figure 1. Generation of the zebrafish models of melanocyte regeneration and melanoma (A) Following NCP treatment, caudal fins of individual zebrafish were collected for each group (control, 1 dpa and 7 dpa) and used as biological replicates (no pooling). **(B)** The zebrafish melanoma model was generated by outcrossing the Tg(*mitfa*-/-; *kita*:GFP-RAS^{G12V}) line with the wt AB zebrafish. 50% of the siblings (*mitfa*+/-) were used as the control group. 50% of the siblings Tg(*mitfa+/-;kita-GFP-RAS^{G12V}*) were used for collection of the nevi and melanoma tissues. Caudal fins were collected for each group and used as biological replicates (no pooling).

Katkat et al., Figure 2

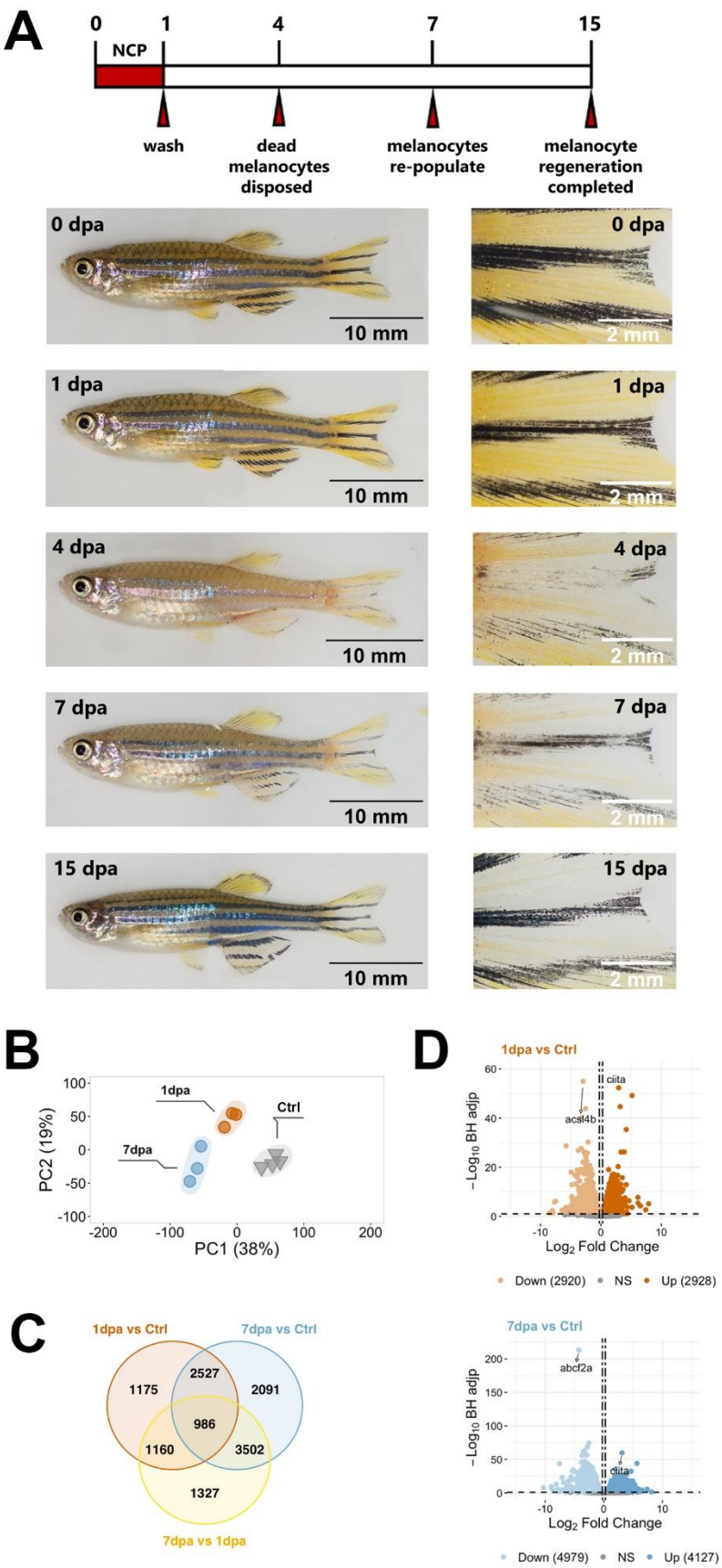

Figure 2. Validation of the melanocyte regeneration model and quantitative analysis of the DEGs at the proliferation and differentiation stages (A) Zebrafish melanocyte regeneration within 15 days after 1 day of NCP treatment. Control zebrafish with normal stripe patterns on the body including the caudal fin prior to NCP treatment (0 dpa). Melanocytes were lost gradually starting at 1 dpa and totally extruded out of the skin at 4 dpa when the stripe pattern was not visible anymore. Melanocytes started to become visible at 7 dpa. At 15 dpa, melanocyte regeneration was completed and the stripe pattern was re-established. Scale bars are 5 mm (whole fish on the left) and 2 mm (close-ups on the right). **(B)** Principal component analysis (PCA) of proliferative (1 dpa) and differentiation (7 dpa) stages of melanocyte regeneration and their controls. Different colors of dots and triangles represent the sample condition. Three sample groups were well clustered among their replicates and well separated from other sample groups. Principal Component 1 (PC1, x-axis) represents 38% and PC2 (y-axis) represents 19% of total variation in the data. **(C)** The Venn diagram shows the number of differentially expressed genes (DEGs) in 1 dpa vs control (orange), 7 dpa vs control (blue), 7 dpa vs 1 dpa (yellow) and the overlap between each set of DEGs of melanocyte regeneration. **(D)** Volcano plots represent changes in gene expression levels in 1 dpa and 7 dpa. Each circle represents a gene. The x-axis shows $\log_2$ of fold change in the condition compared to the control and the vertical dashed lines indicate the fold change cutoffs. The y-axis depicts $-\log_{10}$ of the Benjamini-Hochberg adjusted p-value, where the significance threshold is indicated by a dashed horizontal line. Darker and lighter shades indicate upregulation and downregulation, respectively. dpa: days post-ablation.

Katkat et al., Figure 3

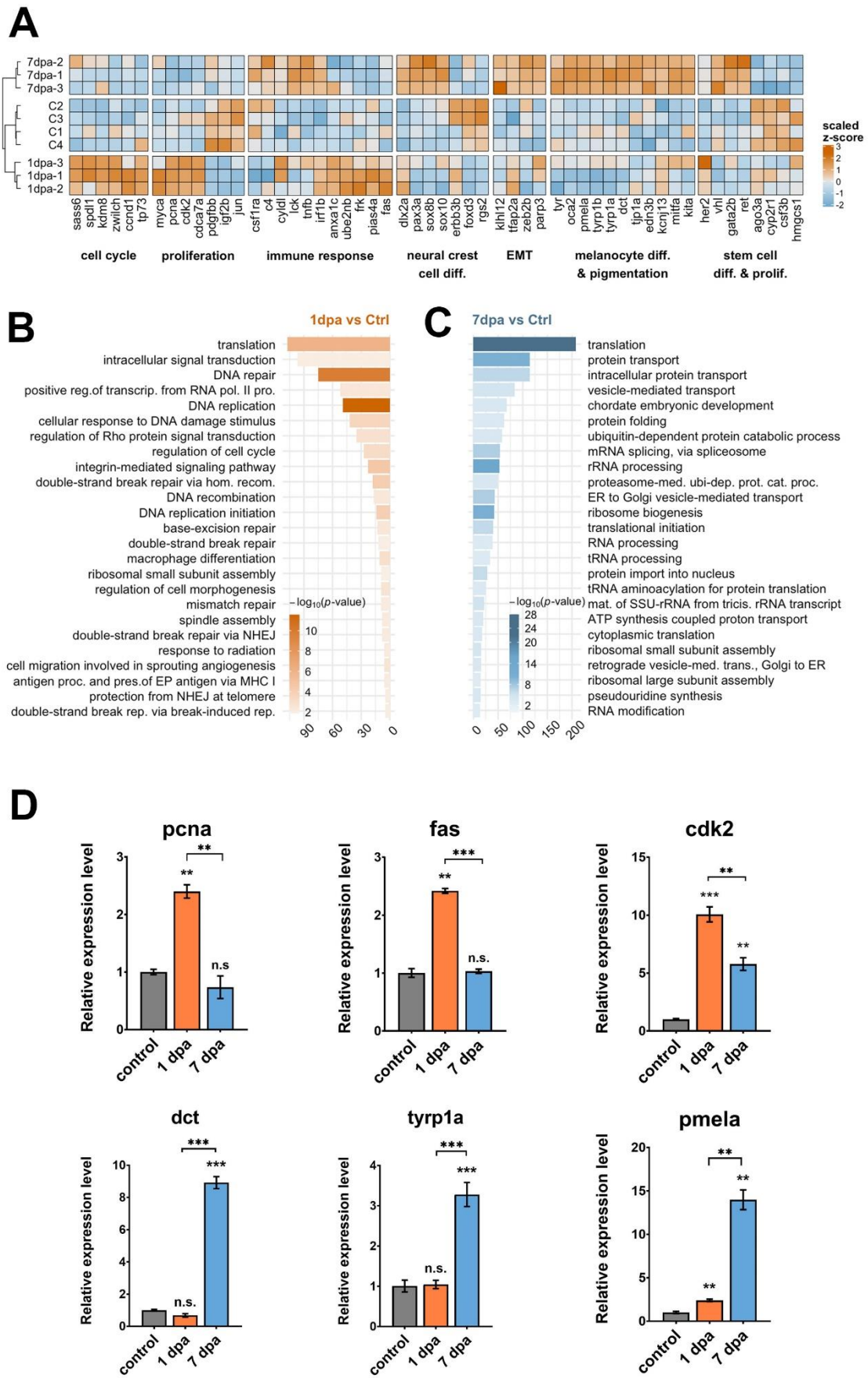

Figure 3. Early and late stages of melanocyte regeneration have distinct gene expression profiles **(A)** The heatmap shows the relative expression of selected genes between proliferation (1 dpa) and differentiation (7 dpa) stages together with the control group. Each column represents a single gene and each row represents a biological replicate of each condition. The scale bar shows z-scores of variance-stabilized (vst-transformed) counts from high to low expression, represented by the color gradient from orange to blue, respectively. **(B-C)** DAVID was used to show the 25 most significantly enriched GO-BP terms based on the transcriptional changes in 1 dpa and 7 dpa comparisons. The color scale shows -$\log_{10}$ of the EASE p-value and x-axis shows the number of genes in each GO-BP term. dpa: days post-ablation, DAVID: Database for Annotation, Visualization, and Integrated Discovery, GO: Gene ontology, BP: Biological process. **(D)** qPCR validations of *pcna*, *fas*, *cdk*, *dct*, *tyrp1a* and *pmela*. *rpl13* was used as the housekeeping control gene. Error bars represent ± standard error of mean (SEM, n=3). Statistical significance was evaluated using unpaired t-test. **$p<0.01$, ***$p<0.001$ and ns: non-significant.

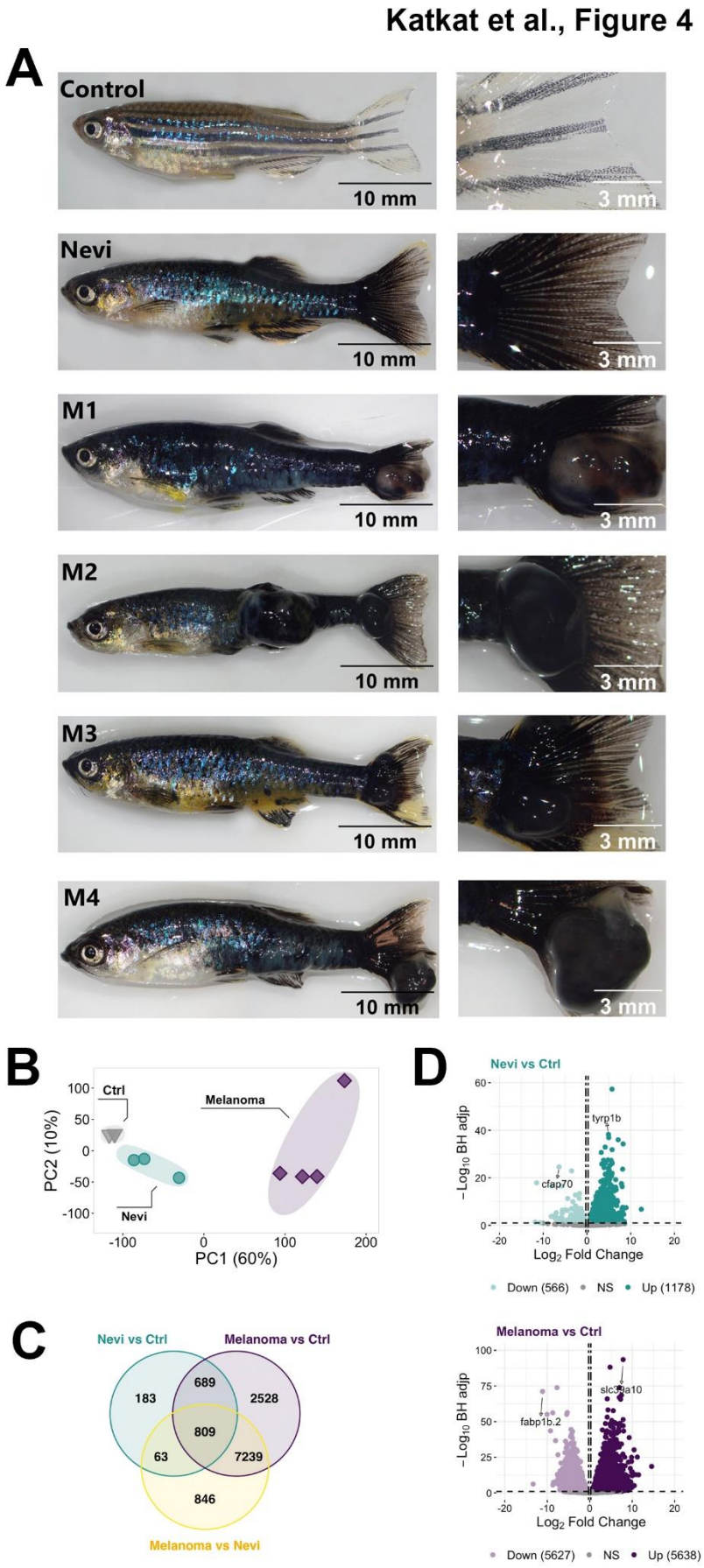
Katkat et al., Figure 4
A
Control
Nevi
M1
M2
M3
M4
10 mm
3 mm
B
Ctrl
Melanoma
Nevi
PC2 (10%)
PC1 (60%)
C
Nevi vs Ctrl
Melanoma vs Ctrl
Melanoma vs Nevi
183
689
2528
809
63
7239
846
D
Nevi vs Ctrl
tyrp1b
cfap70
−Log10 BH adjp
Log2 Fold Change
Down (566)
NS
Up (1178)
Melanoma vs Ctrl
fabp1b.2
slc3a10
Down (5627)
NS
Up (5638)

Figure 4. Validation of the melanoma model and quantitative analysis of the DEGs at the nevi and melanoma stages (A) Zebrafish nevi and melanoma models. The whole fish are shown on the left and their caudal fins that were used for collection of the nevi and melanoma tissue are shown on the right. For melanoma samples, nodular melanoma samples were selected. Tissue materials were collected from the caudal fins of four individuals for each group and used as biological replicates (no pooling). Scale bars are 10 mm (whole fish on the left) and 3 mm (close-ups on the right). **(B)** Principal component analysis (PCA) of nevi, melanoma, and their controls. Different colors of dots and triangles represent the sample condition. Three sample groups were well clustered among their replicates and well separated from other sample groups. Principal Component 1 (PC1, x-axis) represents 60% and PC2 (y-axis) represents 10% of total variation in the data. **(C)** The Venn diagram shows the number of differentially expressed genes (DEGs) in nevi vs control (turquoise), melanoma vs control (purple), melanoma vs nevi (yellow) and the overlap between each set of DEGs. **(D)** Volcano plots represent changes in the gene expression levels in nevi and melanoma. Each circle represents a gene. The x-axis shows $\log_2$ of fold change in the condition compared to the control and the vertical dashed lines indicate the fold change cutoffs. The y-axis depicts $-\log_{10}$ of the Benjamini-Hochberg adjusted p-value, where the significance threshold is indicated by a dashed horizontal line. Darker and lighter shades indicate upregulation and downregulation, respectively.

Katkat et al., Figure 5

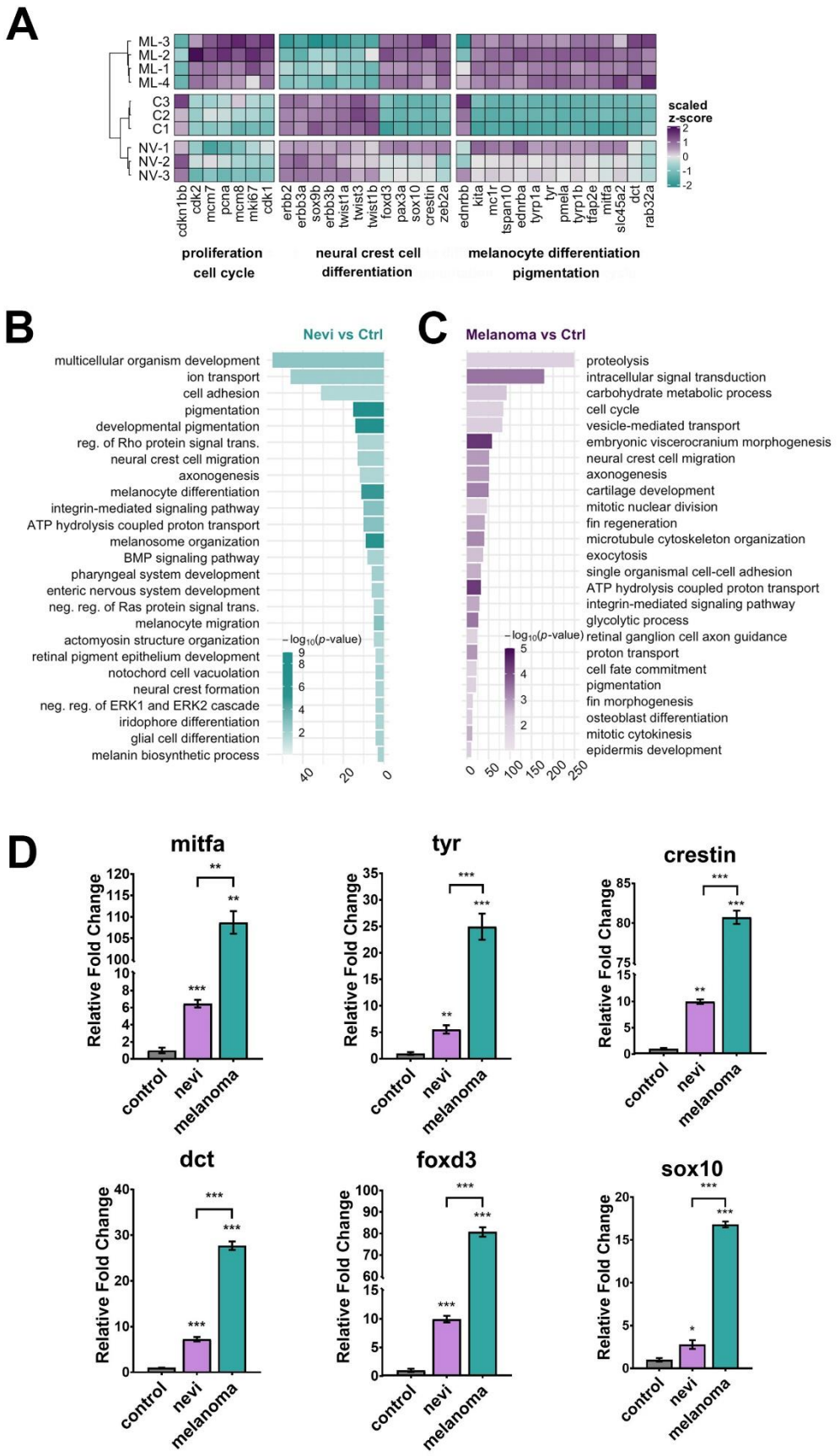

Figure 5. Melanoma resembles melanocytic nevi with respect to the activation of melanocyte differentiation and pigmentation but differs from nevi by the proliferative burst and oppositely regulated NCC signature (A) The heatmap shows the relative expression of selected genes between nevi and melanoma stages together with the control group. Each column represents a single gene, and each row represents a biological replicate of each condition. The scale bar shows z-scores of vst-transformed counts from high to low expression, represented by a color gradient from purple to turquoise, respectively. **(B-C)** DAVID was used to show the 25 most significantly enriched GO-BP terms based on the transcriptional changes in nevi and melanoma comparisons. The color scale shows -$\log_{10}$ of the EASE p-value and the x-axis shows the number of genes in each GO-BP term. DAVID: Database for Annotation, Visualization and Integrated Discovery, GO: Gene ontology, BP: Biological process. **(D)** qPCR validations of *mitfa*, *tyr*, *dct*, *foxd3*, *restin* and *sox10*. *rpl13* was used as the housekeeping control gene. Error bars represent ± standard error of mean (SEM, n=3). Statistical significance was evaluated using unpaired t-test. **$p<0.01$ and ***$p<0.001$.

Katkat et al., Figure 6

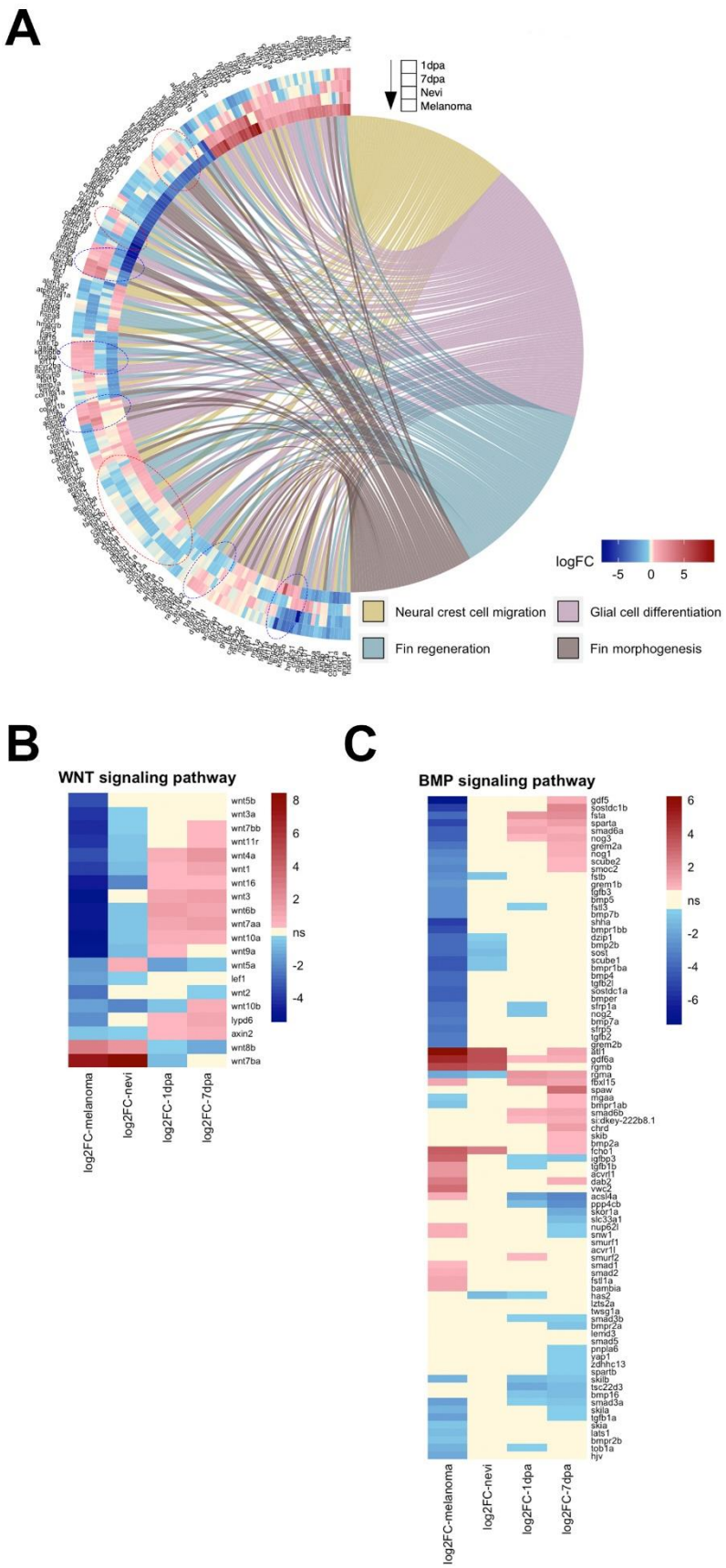

Figure 6. Cellular processes including Wnt and BMP signaling pathways are oppositely regulated during melanocyte regeneration and melanoma (A) GOChord plot shows $\log_2$ fold changes of the genes annotated in selected GO-BP terms for two stages of the melanocyte regeneration, nevi, and melanoma. The genes are linked to their assigned pathways by ribbons and ordered according to their $\log_2$ fold change values from low to high regulation, represented by a color gradient from blue to red, respectively. $\log_2$ fold changes are shown from the outer to the inner annulus in the following order: 1 dpa, 7 dpa, nevi and melanoma. Blue dotted circles show clusters of DEGs that are oppositely regulated between 1 dpa/7 dpa and nevi/melanoma. Red dotted circles show clusters of DEGs that are oppositely regulated between 7 dpa and nevi/melanoma. **(B-C)** Heatmaps of selected genes in Wnt and BMP signaling pathways. Genes and conditions are clustered by similarity of their differential expression profiles ($\log_2$ fold change). $\log_2$ fold change values are represented from high to low regulation by a color gradient from red to blue, respectively. Beige color represents non-significant differential expression (FC<1.2 in both directions or FDR>0.1). dpa: days post ablation.

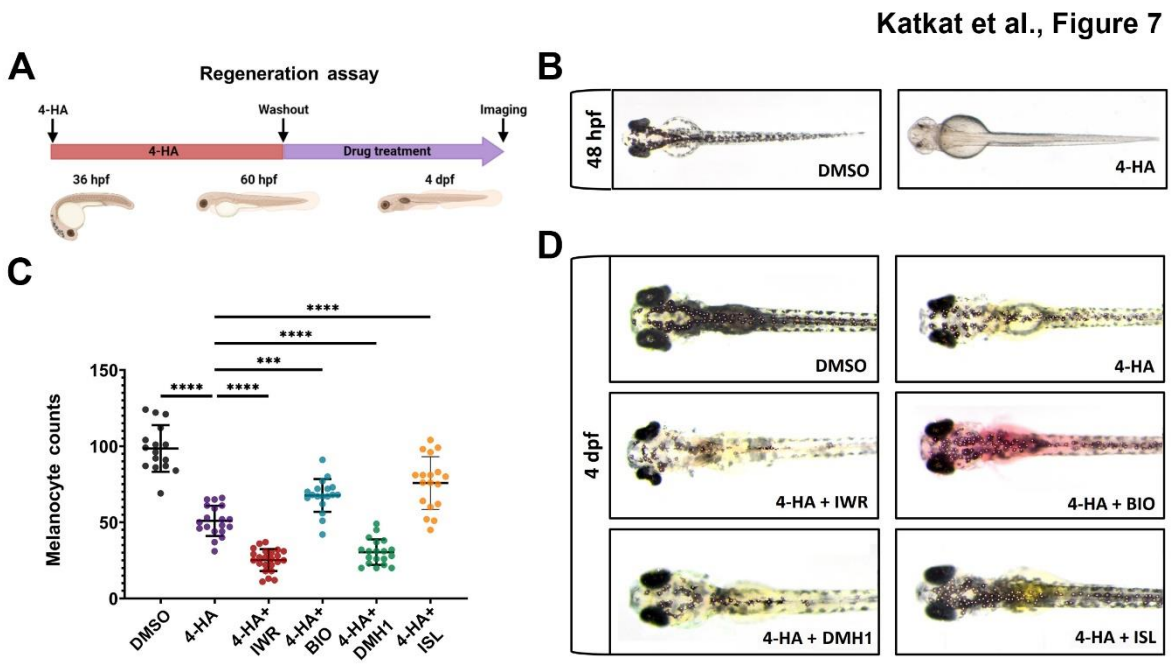

Figure 7. Activation of canonical Wnt or BMP signaling pathways enhances larval melanocyte regeneration (A) Scheme for experimental design of melanocyte regeneration. Zebrafish embryos were treated with 4-HA from 36 hpf to 60 hpf. After washout of 4-HA at 60 hpf, drugs were administered into the embryo water and larvae were analyzed at 4 dpf. **(B)** 2 dpf zebrafish larvae treated with DMSO or 4-HA. **(C)** Dot plot showing the number of melanocytes in 4 dpf larvae treated with DMSO, 4-HA, 4-HA+IWR, 4-HA+BIO, 4-HA+DMH1 or 4-HA+ISL. Each dot represents one larva (DMSO n=16, 4-HA n=19, 4-HA+IWR n=23, 4-HA+BIO n=18, 4-HA+DMH1 n=19, 4-HA+ISL n=17). Statistical significance was evaluated using one-way ANOVA test ***$p < 0.001$, ****$p < 0.0001$. **(D)** Representative images of melanocyte regeneration groups counted in (C).

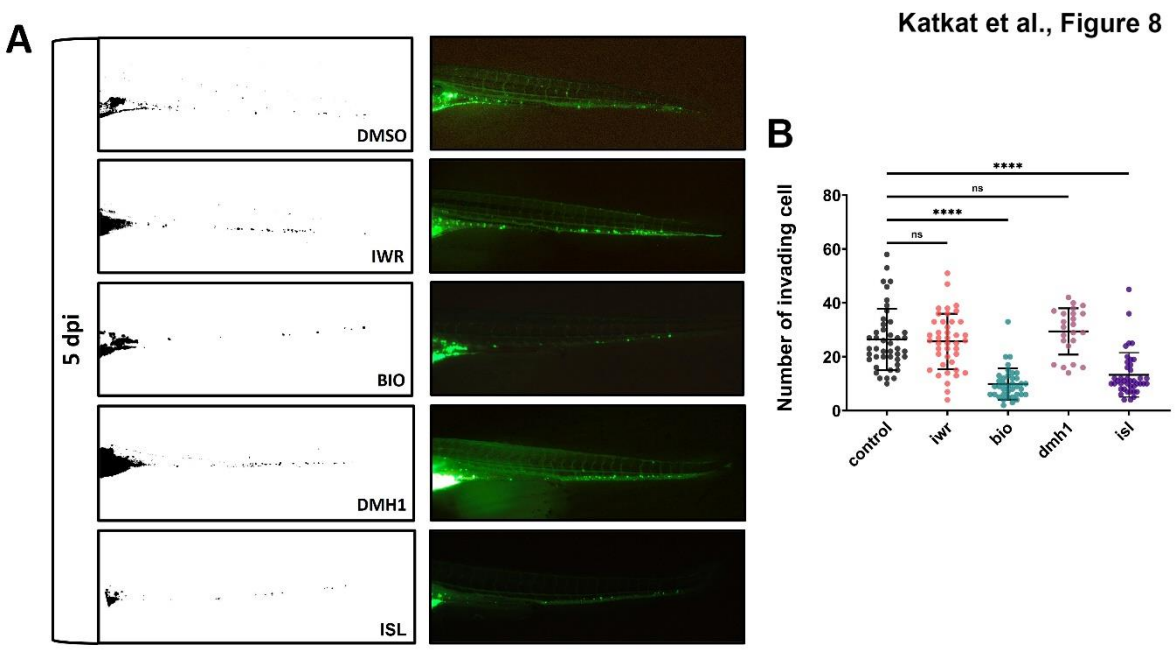

Figure 8. Activation of canonical Wnt or BMP signaling pathways suppresses migration of human melanoma cells (A) Representative fluorescence microscope images of 7 dpf zebrafish embryos injected with human melanoma cells (SK_MEL-28) at 2 dpf and treated with DMSO, IWR, BIO, DMH1 or ISL. **(B)** Dot plot showing the number of invading cells at 7 dpf larval xenografts with micrometastasis. Each dot represents one larval xenograft (DMSO n=44, IWR n=42, BIO n=38, DMH1 n=28, ISL n=41). Statistical significance was evaluated using one-way ANOVA test ****$p < 0.0001$ and ns: non-significant.

Supplementary Figures for Katkat et al.

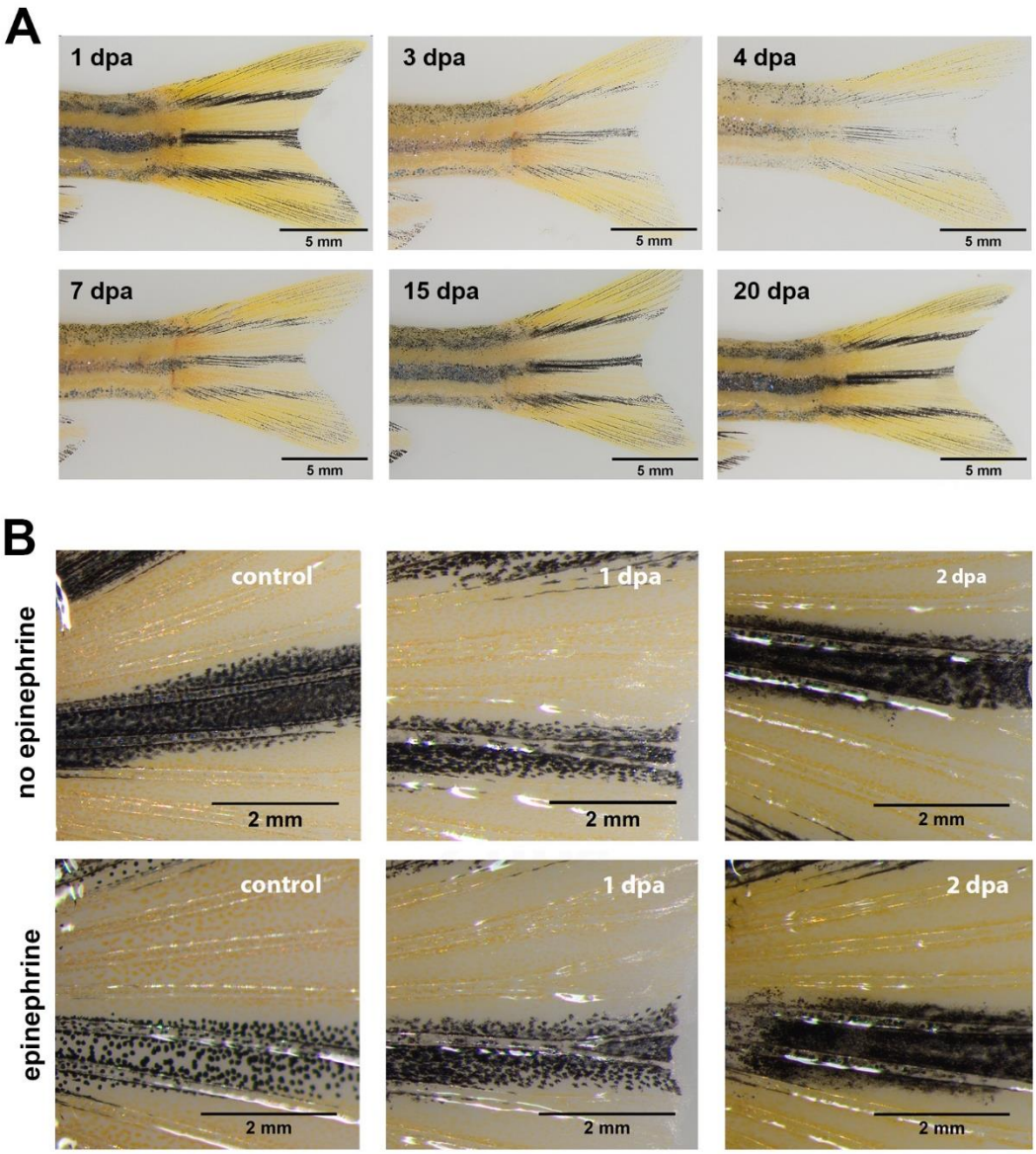

Figure S1. Regeneration and epinephrine response of the zebrafish melanocytes (A) Zebrafish melanocyte regeneration within 20 days after 1 day of NCP treatment. Loss of pigmentation was visible at 3 dpa. Melanocytes were totally disposed out of the skin at 4 dpa. Melanocyte re-pigmentation was detectable at 7 dpa. Scale bars are 5 mm. **(B)** Caudal fins of adult zebrafish following with or without epinephrine treatment. Live melanocytes of the control group rapidly responded to epinephrine by losing their dendritic shape and gathering melanosomes around the nucleus. NCP-treated fish showed no response to epinephrine at 1 dpa and 2 dpa, indicating that their melanocytes were dead and unable to respond. Please note that at 2 dpa, the melanocytes lost their original shape and appeared as black smears. Scale bars are 2 mm.

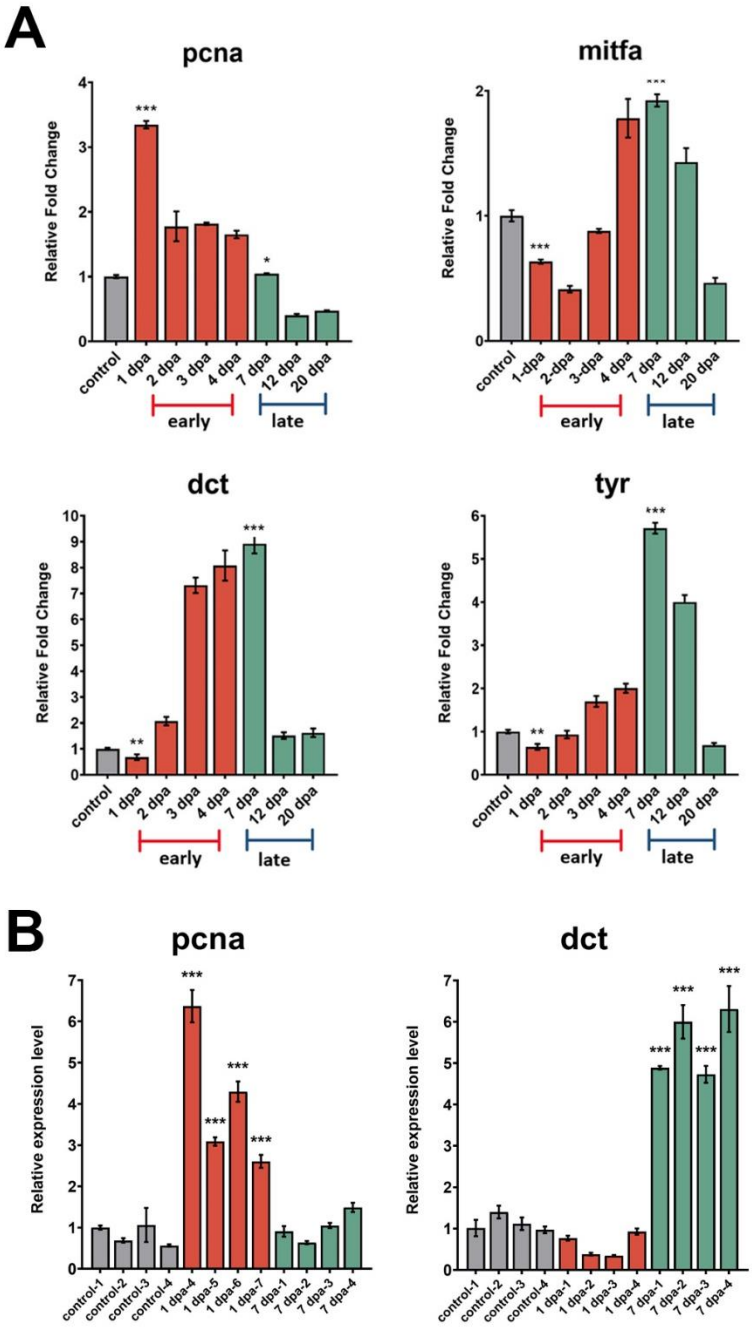

Figure S2. Determination of early and late stages of melanocyte regeneration by qPCR (A) qPCR validations of *pcna*, *mitfa*, *dct* and *tyr* in control and NCP-treated pooled fin samples at 1 dpa, 2 dpa, 3 dpa, 4 dpa, 7 dpa, 12 dpa and 20 dpa. *rpl13* was used as the housekeeping control gene. Error bars represent ± standard error of mean (SEM, n=3). Statistical significance was evaluated using unpaired t-test. *p<0.05, **p<0.01 and ***p<0.001. **(B)** qPCR validations of *pcna* and *dct* in individual control and NCP-treated individual fin samples at 1 dpa and 7 dpa. *rpl13* was used as the housekeeping control gene. Error bars represent ± standard error of mean (SEM, n=3). Statistical significance was evaluated using unpaired t-test. ***p<0.001.

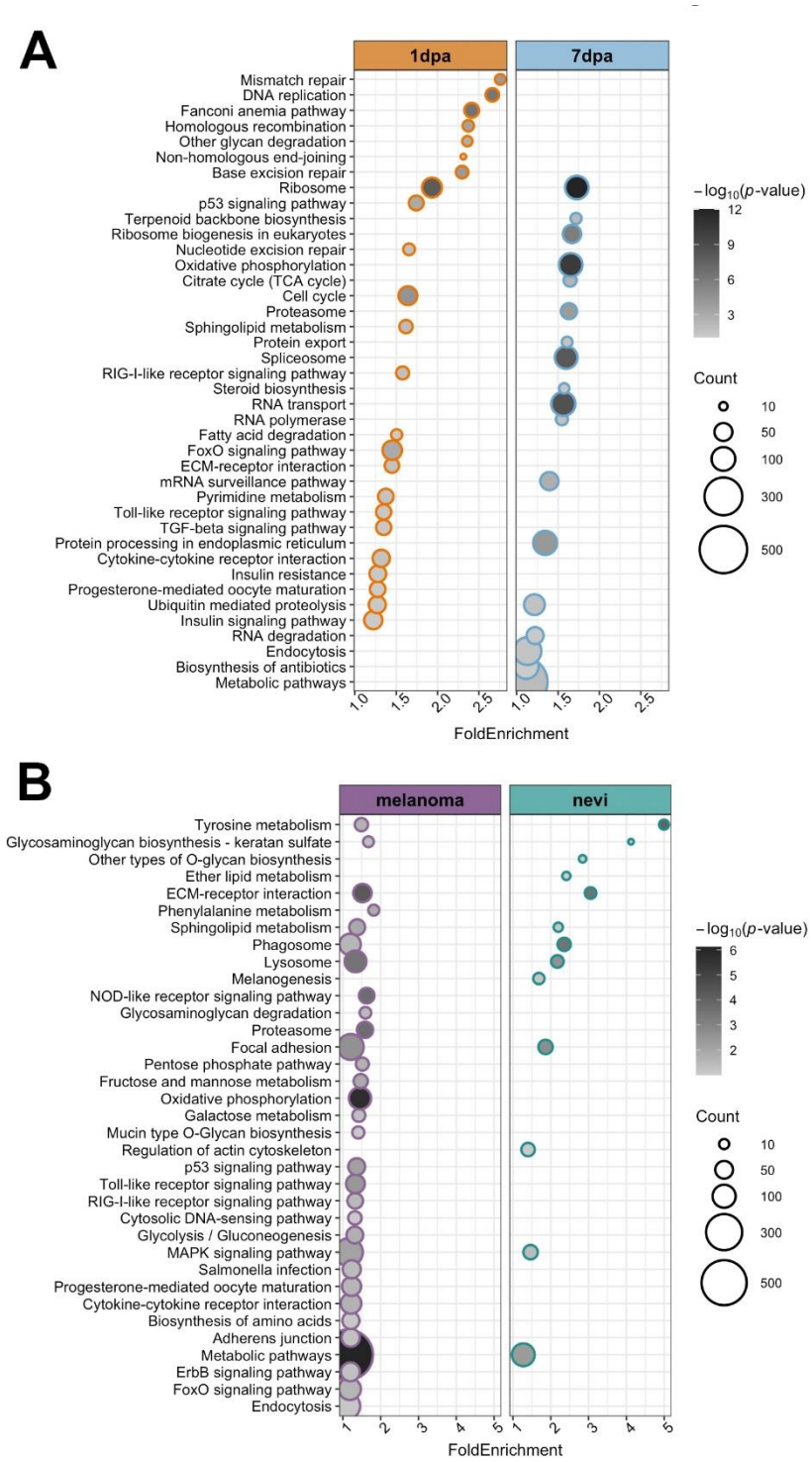

Figure S3. KEGG pathways enriched at two stages of the melanocyte regeneration, nevi, and melanoma determined by using all DEGs. DAVID was used to show the most significantly enriched KEGG pathways based on transcriptional changes at two stages of the melanocyte regeneration **(A)**, nevi, and melanoma **(B)**. All DEGs were used for the analysis. The heatmap's scale shows -$\log_{10}$ of EASE *p*-values for all significantly enriched GO terms. dpa: days post-ablation, DAVID: Database for Annotation, Visualization, and Integrated Discovery, KEGG: Kyoto Encyclopedia of Genes and Genomes.

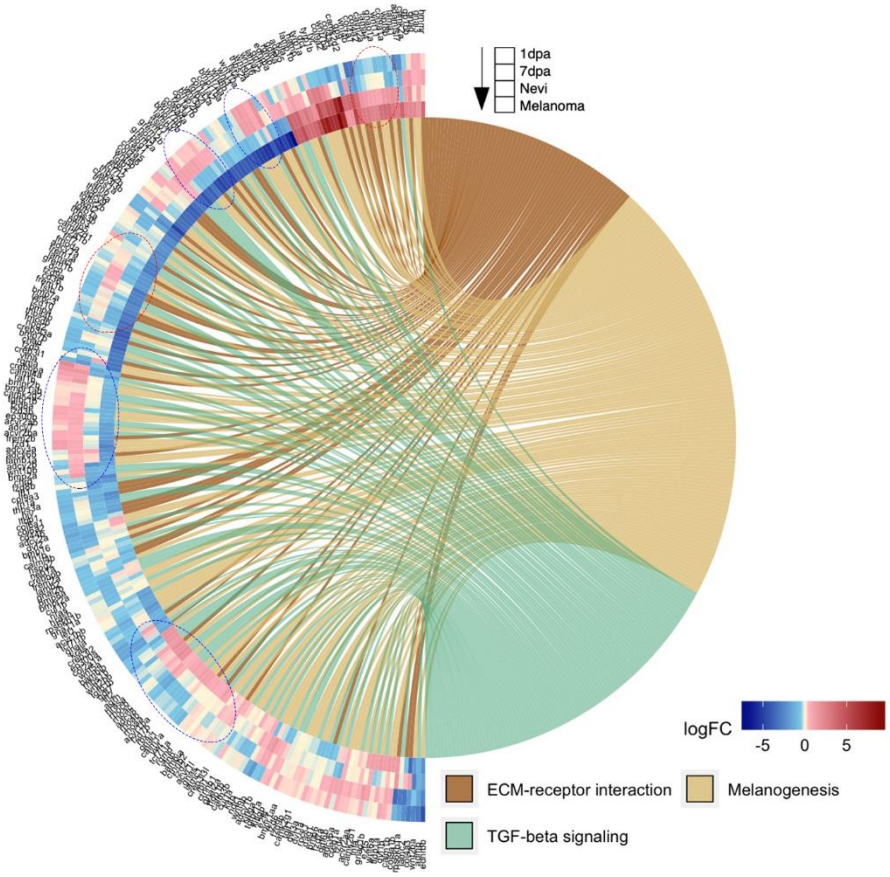

Figure S4. Comparison of 1 dpa, 7 dpa, nevi and melanoma in terms of selected KEGG pathways. GOChord plot shows $\log_2$ fold changes of the genes annotated in selected KEGG pathways for two stages of the melanocyte regeneration, nevi, and melanoma. The genes are linked to their assigned pathways by ribbons and ordered according to their $\log_2$ fold change values from low to high regulation, represented by a color gradient from blue to red, respectively. $\log_2$ fold changes are shown from the outer to the inner annulus in the following order: 1 dpa, 7 dpa, nevi and melanoma. Blue dotted circles show clusters of DEGs that are oppositely regulated between 1 dpa/7 dpa and nevi/melanoma. Red dotted circles show clusters of DEGs that are oppositely regulated between 7 dpa and nevi/melanoma. dpa: days post ablation, KEGG: Kyoto Encyclopedia of Genes and Genomes.

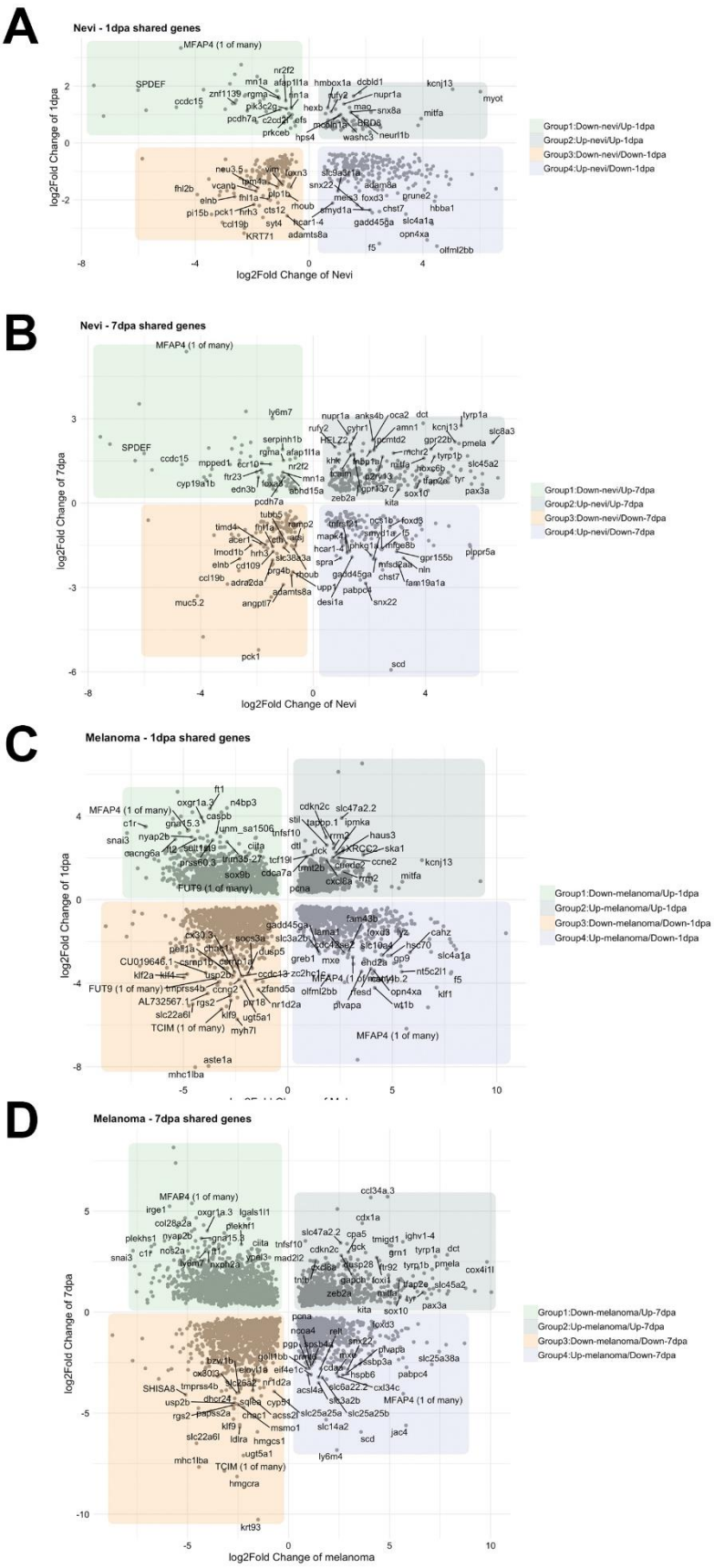
A
Nevi - 1dpa shared genes
log2Fold Change of 1dpa
log2Fold Change of Nevi
Group1:Down-nevi/Up-1dpa
Group2:Up-nevi/Up-1dpa
Group3:Down-nevi/Down-1dpa
Group4:Up-nevi/Down-1dpa
B
Nevi - 7dpa shared genes
log2Fold Change of 7dpa
log2Fold Change of Nevi
Group1:Down-nevi/Up-7dpa
Group2:Up-nevi/Up-7dpa
Group3:Down-nevi/Down-7dpa
Group4:Up-nevi/Down-7dpa
C
Melanoma - 1dpa shared genes
log2Fold Change of 1dpa
Group1:Down-melanoma/Up-1dpa
Group2:Up-melanoma/Up-1dpa
Group3:Down-melanoma/Down-1dpa
Group4:Up-melanoma/Down-1dpa
D
Melanoma - 7dpa shared genes
log2Fold Change of 7dpa
log2Fold Change of melanoma
Group1:Down-melanoma/Up-7dpa
Group2:Up-melanoma/Up-7dpa
Group3:Down-melanoma/Down-7dpa
Group4:Up-melanoma/Down-7dpa

Figure S5. Identification of shared DEGs in two stages of melanocyte regeneration, nevi and melanoma. The 4-direction scatter plot shows differentially expressed genes (DEGs) shared between **(A)** nevi and 1 dpa, **(B)** nevi and 7 dpa, **(C)** melanoma and 1 dpa, and **(D)** melanoma and 7 dpa. Only significantly changed genes were included (Table S2). Shared DEGs were split into 4 groups based on their log fold change between conditions: Group1 genes were downregulated in nevi/melanoma but upregulated in 1 dpa/7 dpa (light green). Group2 genes were upregulated in nevi/melanoma but downregulated in 1 dpa/7 dpa (light blue). Group3 genes were downregulated in both nevi/melanoma and in 1 dpa/7 dpa (light orange). Group4 genes were upregulated in both nevi/melanoma and in 1 dpa/7 dpa (light purple).